HHS Public Access

Author manuscript

Cell Rep. Author manuscript; available in PMC 2021 August 02.

Published in final edited form as:

Cell Rep. 2021 July 13; 36(2): 109363. doi:10.1016/j.celrep.2021.109363.

Extracellular domain shedding of the ALK receptor mediates neuroblastoma cell migration

Hao Huang[1,2], **Alexander Gont**[3], **Lynn Kee**[3], **Ruben Dries**[1,2], **Kathrin Pfeifer**[4], **Bandana Sharma**[1,2], **David N. Debruyne**[1,2], **Matthew Harlow**[1,2], **Satyaki Sengupta**[1,2], **Jikui Guan**[4], **Caleb M. Yeung**[1,2], **Wenchao Wang**[1,2], **Bengt Hallberg**[4], **Ruth H. Palmer**[4], **Meredith S. Irwin**[3,*], **Rani E. George**[1,2,5,*]

[1]Department of Pediatric Hematology/Oncology, Dana-Farber Cancer Institute, Boston, MA 02215, USA

[2]Department of Pediatrics, Harvard Medical School, Boston, MA 02115, USA

[3]Department of Pediatrics and Cell Biology Program, The Hospital for Sick Children, University of Toronto, Toronto, ON, Canada

[4]Department of Medical Biochemistry and Cell Biology, Institute of Biomedicine, Sahlgrenska Academy, University of Gothenburg, Gothenburg, Sweden

[5]Lead contact

SUMMARY

Although activating mutations of the anaplastic lymphoma kinase (ALK) membrane receptor occur in ~10% of neuroblastoma (NB) tumors, the role of the wild-type (WT) receptor, which is aberrantly expressed in most non-mutated cases, is unclear. Both WT and mutant proteins undergo extracellular domain (ECD) cleavage. Here, we map the cleavage site to Asn654-Leu655 and demonstrate that cleavage inhibition of WT ALK significantly impedes NB cell migration with subsequent prolongation of survival in mouse models. Cleavage inhibition results in the downregulation of an epithelial-to-mesenchymal transition (EMT) gene signature, with decreased nuclear localization and occupancy of β-catenin at EMT gene promoters. We further show that cleavage is mediated by matrix metalloproteinase 9, whose genetic and pharmacologic inactivation inhibits cleavage and decreases NB cell migration. Together, our results indicate a pivotal role for WT ALK ECD cleavage in NB pathogenesis, which may be harnessed for therapeutic benefit.

*Correspondence: meredith.irwin@sickkids.ca (M.S.I.), rani_geoge@dfci.harvard.edu (R.E.G.).

AUTHOR CONTRIBUTIONS

R.E.G. conceived the project and supervised the research. R.E.G. and H.H. designed the experiments. H.H. planned and performed the molecular, cellular, and biochemical studies. A.G. and L.K. performed mouse experiments under the supervision of M.S.I. H.H., D.N.D., and R.D. analyzed the microarray expression data. B.S. and C.M.Y. provided technical assistance. W.W., M.H., and S.S. generated plasmid constructs and performed certain experiments. J.G. designed and generated the *Drosophila* constructs. K.P. performed the *Drosophila* experiment under the supervision of B.H. and R.P. R.E.G. and H.H. wrote the manuscript with feedback from all authors.

SUPPLEMENTAL INFORMATION

Supplemental information can be found online at https://doi.org/10.1016/j.celrep.2021.109363.

DECLARATION OF INTERESTS

The authors declare no competing interests.

Graphical abstract

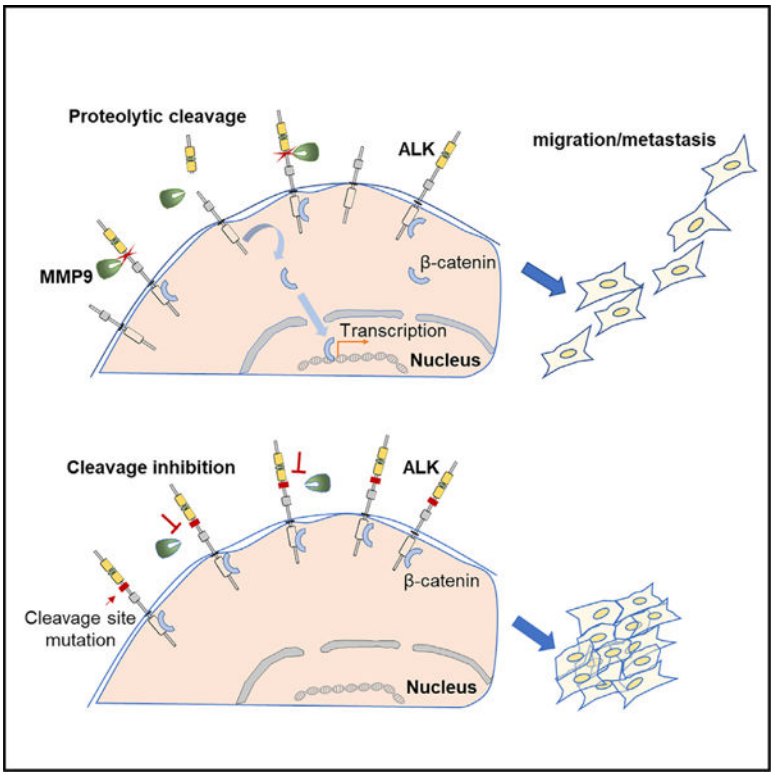

In brief

Huang et al. show that extracellular domain (ECD) cleavage of the ALK cell surface tyrosine kinase receptor mediates neuroblastoma cell migration through induction of an EMT phenotype. ECD cleavage is caused by MMP-9 whose inhibition leads to decreased cell migration.

INTRODUCTION

Aberrant expression of the ALK membrane receptor is driven by point mutations, amplification, or protein fusions and provides a tractable therapeutic target in cancers in which these mutant proteins contribute to the malignant phenotype (Hallberg and Palmer, 2016). NB, a tumor of the sympathetic nervous system arising from the neural crest, affords an excellent example; the identification of activating mutations of the *ALK* gene have led to clinical trials of ALK inhibitors in this subgroup of patients (Chen et al., 2008; George et al., 2008; Janoueix-Lerosey et al., 2008; Mossé et al., 2008). Such lesions, occurring in approximately 10% of tumors, are located primarily in the intracellular kinase domain of ALK, leading to its constitutive phosphorylation and activation of downstream signaling pathways that induce abnormal cell proliferation. In addition, the WT ALK receptor, expressed almost exclusively in the developing nervous system, where it facilitates apoptosis through caspase-mediated cleavage of its intracytoplasmic segment (Mourali et al., 2006), is overexpressed in almost 90% of NB tumors (Lamant et al., 2000; Passoni et al., 2009). However, the role of WT ALK, if any, in tumorigenesis is unclear, although certain

observations suggest that it may contribute to the cancer phenotype. First, increased WT ALK expression in NB correlates with a poor patient outcome (De Brouwer et al., 2010; Passoni et al., 2009; Schulte et al., 2011). Second, activation of WT ALK has been linked to the proliferation, migration, and invasion of NB cells and downstream signaling in HEK293 and PC12 pheochromocytoma cells (Hasan et al., 2013; Moog-Lutz et al., 2005; Motegi et al., 2004; Souttou et al., 2001). Third, depletion of WT ALK expression in NB cell lines causes growth arrest and cell death (Di Paolo et al., 2011; Mossé et al., 2008; Passoni et al., 2009). These results suggest that, in most NB tumors in which ALK is overexpressed, mechanisms other than DNA alterations lead to its aberrant function and may, therefore, contribute to the pathophysiology of the tumor.

In NB cell lines and primary tumors, the ALK protein is expressed as a 220-kDa form, representing the heavily glycosylated, full-length membrane receptor and as a shorter 140-kDa product, resulting from cleavage or shedding of the N-terminal ECD (Moog-Lutz et al., 2005; Osajima-Hakomori et al., 2005). The significance of such ECD shedding is unknown; structural alterations that remove the ECD-encoding exons 1–4, some of which lead to ALK activation (Okubo et al., 2012; Souttou et al., 2001), have been reported in NB cell lines and 2.4% of primary tumors (Brady et al., 2020; Cazes et al., 2013; Fransson et al., 2015; Okubo et al., 2012), suggesting a repressor role for this domain. Additionally, culture of NB cells in Schwann cell medium abolished ALK ECD cleavage (Degoutin et al., 2009), consistent with the differentiated nature and excellent patient outcome of Schwannian-stroma-rich tumors compared with their stroma-poor counterparts (Shimada et al., 1984). These findings led us to hypothesize that shedding of the ALK ECD contributes to the malignant phenotype of NB cells. To pursue that notion, we undertook studies to identify the ALK ECD cleavage site, the mechanism(s) responsible for cleavage as well as the functional consequences of this modification in NB.

RESULTS

ALK ECD cleavage generates a shed ectodomain and a membrane-bound fragment

The full-length ALK receptor comprises an extracellular, a transmembrane, and an intracellular domain (Figure 1A). The ECD, which contains binding sites for the ALK ligands ALKAL1 and ALKAL2, (FAM150A/B) (Guan et al., 2015) and Augα/β (Reshetnyak et al., 2015), consists of an N-terminal signal peptide, two meprin-A5-protein receptor tyrosine phosphatase Mμ (MAM) domains separated by a low-density lipoprotein class A motif (LDLa), and a glycine-rich region, whereas the intracellular domain includes a catalytic protein tyrosine kinase domain (Iwahara et al., 1997). To verify the existence of ALK cleavage in NB cells, we first analyzed human NB cell lines using an antibody directed to the C-terminal domain of ALK, which revealed both the 220-kDa full-length receptor and the 140-kDa products (Figure 1B). The two protein products were identified in all NB cells that expressed ALK, irrespective of ALK-mutation status. ALK ECD cleavage was also apparent in patient-derived xenograft (PDX) NB models (Figure 1C). Consistent with the highest expression of ALK occurring during development (Iwahara et al., 1997; Morris et al., 1994), the two ALK fragments were also observed in neonatal murine brain tissue (Figure 1D). To ensure that the 140-kDa fragment resulted from proteolytic cleavage of the

full-length receptor, we used 8G7, an N-terminal ALK monoclonal antibody that binds to the ECD of human ALK with high specificity, to analyze conditioned media from NB cell lines. An ALK fragment with a molecular mass of approximately 100 kDa was identified in the conditioned media of all five NB cell lines whose lysates were positive for the full-length 220-kDa and the truncated 140-kDa products, confirming ectodomain shedding (Figure 1E). Consistent with this finding, the 8G7 antibody detected the 220-kDa full-length protein but not the 140-kDa fragment in cell lysates (Figure 1E). Thus, ECD shedding is common to both WT and mutated ALK, is conserved across malignant and non-malignant tissue contexts, and is an integral feature of the ALK receptor.

ECD cleavage occurs between the MAM2 domain and the glycine-rich region of ALK

To identify the ECD cleavage site, we used the 8G7 N-terminal antibody to isolate the shed ALK fragment by immunoprecipitation from conditioned media of NGP human NB cells that endogenously express both full-length and cleaved WT ALK (Figures 1E and S1A). The purified ECD protein was then enzymatically digested with chymotrypsin and subjected to high-performance liquid chromatography (HPLC)-tandem mass spectrometry (LC-MS/MS). As expected, chymotrypsin digestion yielded several peptides whose C termini corresponded to the YWFL (tyrosine, tryptophan, phenylalanine, and leucine) consensus site for chymotrypsin digestion. However, another peptide, ending at asparagine 654 (N or Asn654), ^{636}LTISGEDKILQN-TAPKSRN^{654}, was also identified in two fully independent replicates (Figures 1F, S1B, and S1C). Because this residue is not a typical chymotrypsin-digestion site, we surmised that Asn654 could be the natural ECD cleavage site. To prove that was the case, we digested the ECD protein with trypsin. Trypsin digestion generated peptides that terminated at the consensus trypsin digestion site (lysine [K] or arginine [R]), one of which, ^{644}ILQNTAPK^{651}, was located N-terminal to the putative ALK ECD cleavage site at Asn654 and which corresponds to part of the same fragment that was identified in the chymotrypsin digest (Figures 1F, S1D, and S1E). The similar molecular weights of an engineered ALK ECD construct (ALK1–654) expressed in 293T cells (which do not endogenously express ALK) and the shed ALK fragment (Figure 1G) supports this interpretation. The putative cleavage site and its consensus sequence are highly conserved across mammalian species (Figure S1F), suggesting an essential role for ECD cleavage in ALK-expressing cells.

To verify the identity of our proposed cleavage site, we generated several cleavage-site mutants (CSMs; Figure S2A) and examined their cleavage efficiencies when overexpressed in 293T cells (Figure 1H). As a positive control, we used WT ALK, which undergoes cleavage when expressed in these cells; the negative control was the ALK Δ638–682 construct, which contains a 45 aa deletion C-terminal to the MAM2 domain and does not undergo cleavage. All the CSM constructs showed varying degrees of cleavage inhibition, with deletions or mutations of the amino acids at positions 655 and 656 identified as the minimum changes required for cleavage inhibition (Figures 1H and S2B). Similar results were observed in NIH 3T3 cells, which lack endogenous ALK expression but were engineered to express WT and CSM proteins (Figure S2C). Using biotinylation assays, we confirmed that the CSMs, especially ALK LF655del when overexpressed in 293T cells, were presented to the cell membrane, thereby enabling further functional studies (Figures 1I

and S2D). Similar to WT ALK, the ALK LF655del CSM was able to homo- and heterodimerize with the WT receptor (Figure S3A) and exhibited similar kinase activity (Figure S3B). When overexpressed in NIH 3T3 cells, ALK LF655del showed decreased phosphorylation and downstream signaling compared with WT ALK (Figure S3C). The ALK ligands ALKAL1 and ALKAL2 (Guan et al., 2015; Reshetnyak et al., 2015), which bind to the glycine-rich region C-terminal of the putative cleavage site, upregulated ALK LF655del phosphorylation but to a much lesser extent than that of WT ALK (Figure S3D). Similar results were observed when the CSMs were tested in the *Drosophila* eye model (Figure S3E). Considered together, these results confirm Asn654-Leu655 as the ECD cleavage site of ALK and demonstrate that cleavage inhibition retains the intrinsic properties of the WT receptor, albeit at decreased levels.

The LF655del mutation inhibits ALK cleavage in NB cells

To investigate the functional effects of ALK ECD cleavage in the NB cell context, we used CRISPR-Cas9-mediated editing to introduce the LF655del mutation into the endogenous ALK locus in NGP NB cells that overexpress full-length WT ALK that undergoes spontaneous ECD cleavage. Single-cell selection yielded the $NGP^{ALK(LF655del)}$ knock-in clone; in which, biallelic editing was confirmed by sequencing (Figure 2A). $NGP^{ALK(LF655del)}$ cells appeared to be morphologically different from $NGP^{CRISPR\ ctrl}$ (cells expressing a control editing vector) cells and tended to adhere together in clumps (Figure 2B). $NGP^{ALK(LF655del)}$ cells exhibited a predominance of the 220-kDa full-length protein, with the 140 kDa truncated form being absent or present at extremely low levels, an effect that could be rescued by overexpression of WT ALK (Figure 2C). In addition, the shed ALK ECD fragment was absent in conditioned media from these cells, confirming inhibition of cleavage (Figure 2D). Phosphorylation of the 220-kDa full-length band was similar in $NGP^{ALK(LF655del)}$ and $NGP^{CRISPR\ ctrl}$ cells, and unlike NIH 3T3 cells, in which the ALK LF655del CSM was ectopically expressed, $NGP^{ALK(LF655del)}$ cells showed no differences in downstream signaling pathways (Figure 2D). We also ascertained that the CRISPR-edited ALK receptor was still expressed at the NGP cell membrane through immunofluorescence assays (Figure 2E) and that it was glycosylated (Figure S4A). To ensure that these results were not unique to a single NB cell line or the method of cleavage inhibition, we overexpressed WT and the uncleavable ALK LF655del CSM in SK-N-AS and CHP-212 human NB cells which normally express very low levels of ALK (Figure S4B). After ascertaining cell surface expression, we determined that ALK WT underwent ECD cleavage in these cells, whereas the LF655del CSM failed to do so (Figures S4C and S4D). Again, no differences in downstream signaling were observed between cells expressing the cleaved and uncleavable proteins, suggesting that ALK cleavage does not affect signaling in these tumor cells that already possess established canonical signaling pathways.

Inhibition of ALK ECD shedding limits the migration of NB cells

To determine whether ALK ECD shedding had a functional role in NB, we first assessed the effect of cleavage inhibition on cell growth. Uncleavable ALK-expressing $NGP^{ALK(LF655del)}$ cells exhibited no changes in cell growth or cell cycle progression as compared with $NGP^{CRISPR\ ctrl}$ cells (Figures S4E–S4G). Given prior reports of the role of WT ALK in the migration and invasion of NB cells (Hasan et al., 2013), we next determined whether ECD

cleavage featured in these processes. $NGP^{ALK(LF655del)}$ cells exhibited a 3-fold reduction in migration compared with $NGP^{CRISPR\ ctrl}$ cells (Figure 3A), which could be rescued by overexpression of cleavable WT ALK. Inhibition of ECD cleavage also decreased the invasion and wound healing capacities of $NGP^{ALK(LF655del)}$ cells compared with $NGP^{CRISPR\ ctrl}$ cells (Figures 3B and 3C). Similar to the effects on migration, these deficits were also overcome by the ectopic expression of WT ALK in these cells. We also analyzed these effects in additional non-transformed and human NB cells engineered to express WT or LF655del ALK and observed that the former led to potentiation of cell migration and invasion, whereas the latter had no effect on these processes (Figures 3D, 3E, S5A, and S5B). We next considered whether the effects on cell migration were mediated by the truncated membrane-bound ALK receptor that remains after ECD cleavage. We, therefore, overexpressed the ALK 655–1604 fragment together with an N-terminal membrane-localizing signal peptide (Hallberg and Palmer, 2016) in SK-N-AS and CHP-212 NB cells. After verifying that ALK 655–1604 was presented to the cell membrane (Figure S4C), we determined that overexpression of this fragment did not recapitulate the enhanced cell migration observed with cleaved WT ALK (Figures 3D and 3E). Similarly, incubation of $NGP^{ALK(LF655del)}$ or CHP-212 NB cells that ectopically expressed the ALK LF655del or ALK 655–1604 proteins in conditioned media containing the shed ALK (ALK 1–654) ECD fragment had no effect on migration potential (Figures S5C and S5D). These results suggest that ALK ECD cleavage contributes to the migratory and invasive properties of cells that express WT ALK. Additionally, it appears that the cleavage process itself, rather than the truncated or shed fragments, mediate these processes.

Finally, to determine whether ALK ECD cleavage has a functional role in NB cells expressing gain-of-function ALK mutations, we introduced an ALK cleavage-site mutation into Kelly NB cells that endogenously express the F1174L kinase mutation (George et al., 2008) through CRISPR editing (Figures S6A and S6B). Migration, invasion, and wound healing were not affected in these cells (Figures S6C–S6E), likely because the constitutive kinase activity of ALK F1174L has a dominant role in mediating cell motility, which overcomes the effects caused by ALK ECD cleavage inhibition.

Inhibition of ALK ECD cleavage decreases NB cell migration in animal models

To substantiate the apparent role of ALK cleavage in NB cell migration *in vivo*, we next compared the migratory potential of $NGP^{ALK(LF655del)}$ NB cells in which ALK ECD cleavage was endogenously inhibited versus those in which WT ALK was cleaved ($NGP^{CRISPR\ ctrl}$). We used an intracardiac murine model of NB metastasis in which cells migrate to the bone marrow and bone with high penetrance, similar to the pattern of NB spread in patients (Seong et al., 2017). Luciferase-labeled cells were injected into 9-week-old non-obese diabetic/severe combined immunodeficiency (NOD/SCID) mice and monitored for evidence of spread using bioluminescence imaging. At day 35 after injection, the latest time point at which each group had an equal number of animals, mice in which $NGP^{ALK(LF655del)}$ cells were introduced showed significant decreases in the total metastatic burden compared with mice injected with $NGP^{CRISPR\ ctrl}$ cells (Figures 4A and 4B). Between days 35 and 82 after cell injection, all $NGP^{CRISPR\ ctrl}$ tumor mice had to be euthanized because of widespread disease in comparison to $NGP^{ALK(LF655del)}$ animals that

required euthanasia between 52 and 108 days. Thus, there was a delay in metastatic colonization (35 versus 52 days) of tumor cells expressing uncleavable ALK. Importantly, the animals in which ALK ECD cleavage was inhibited showed a significant increase in survival (Figure 4C). As previously described for the intracardiac model of NB cell metastasis (Seong et al., 2017), NB cells migrated to the bone marrow/bone and adrenal glands, with no difference in metastatic sites between the two groups. To ensure that our results were not due to the method of *in vivo* tumor generation, we also tested the metastasis-forming ability of $NGP^{ALK(LF655del)}$ and $NGP^{CRISPR\ ctrl}$ xenograft models generated through tail vein injection (Figure 4D). This *in vivo* study recapitulated the significantly reduced metastatic potential of $NGP^{ALK(LF655del)}$ cells. At day 42 after injection, mice that had received $NGP^{ALK(LF655del)}$ cells showed significantly decreased tumor burden compared with that of controls. Finally, we also tested the effect of ALK cleavage on cell metastasis in an additional NB mouse model using SK-N-AS NB cells ectopically expressing either WT or LF655del ALK (Figure 4E). Tumor xenograft models derived from intracardiac injection of luciferase-labeled SK-N-AS cells expressing LF655del showed significantly decreased metastasis compared with that of WT ALK-expressing control animals. These *in vivo* results indicate a key role for ALK ECD cleavage in NB cell migration.

ALK ECD cleavage leads to an EMT gene expression signature

Given the absence of signaling alterations in ALK cleavage-inhibited cells, we next sought alternative mechanisms to explain the observed defects in migration by first comparing the gene expression profiles of $NGP^{ALK(LF655del)}$ with those of $NGP^{CRISPR\ ctrl}$ cells. Although most transcripts were unchanged between the two cell types (Figure 5A), gene set enrichment analysis (GSEA) showed significant enrichment for genes involved in EMT in $NGP^{ALK(LF655del)}$ cells (Figure 5B), with these genes featuring prominently among the most downregulated transcripts (Figures 5C and 5D). Gene ontology (GO) analysis identified genes involved in neuronal migration as the most-enriched category (Figure 5E). The downregulated EMT signature was also reflected in the protein expression levels of candidate genes with key roles in EMT (Lamouille et al., 2014) (Figure 5F). Hence, inhibition of ALK ECD cleavage contributed to the loss of an EMT signature, thereby leading to effects on cell migration.

The Wnt/β-catenin signaling pathway is one of the key modulators of EMT (Thiery et al., 2009; Valenta et al., 2012). In addition to its role in signaling, β-catenin is normally sequestered and stabilized at the cell membrane as a structural component of cadherin-based adherence junctions (Meng and Takeichi, 2009). Release of β-catenin from its binding partners can lead to its nuclear translocation, where it drives the expression of target genes, including those involved in EMT regulation. Interestingly, β-catenin was recently found to bind to the intracellular domain of ALK, causing steric hindrance to ALK-inhibitor binding and subsequent resistance to therapy (Alshareef et al., 2016, 2017). This evidence, together with our observation that the top differentially downregulated genes in $NGP^{ALK(LF655del)}$ cells included targets of β-catenin involved in EMT (Figures 5C and 5D), led us to question its role in mediating the migratory effects of ALK ECD cleavage. Co-immunoprecipitation assays showed that β-catenin binds to the intracellular domain of WT ALK and that binding

is retained when ECD cleavage is inhibited (Figure 6A). On the other hand, binding of β-catenin to the truncated membrane-bound ALK 655–1604 receptor was significantly reduced, suggesting that ECD cleavage releases β-catenin from ALK, thereby enabling it to be transported to the nucleus. In support of this prediction, decreased levels of nuclear versus cytoplasmic β-catenin were observed in $NGP^{ALK(LF655del)}$ cells compared with untransfected NGP or $NGP^{CRISPR\ ctrl}$ cells (Figures 6B and 6C). Furthermore, phosphorylation of β-catenin at serines 552 and 675, which helps to maintain the stability of the protein and enables transcriptional co-activator binding (van Veelen et al., 2011), was decreased in $NGP^{ALK(LF655del)}$ cells, prompting us to analyze β-catenin function in the nucleus (Figure 6D). Chromatin immunoprecipitation (ChIP)-qPCR analysis revealed significantly diminished occupancies of β-catenin and its nuclear partner TCF-4, at the promoters of EMT genes, fibronectin 1 (*FN1)* (Zirkel et al., 2013), *PITX2* (Kioussi et al., 2002), and *COL3A1* (Xiang et al., 2017) in $NGP^{ALK(LF655del)}$ cells compared with that of $NGP^{CRISPR\ ctrl}$ cells (Figure 6E). Taken together, these results suggest that ALK ECD shedding could contribute to NB cell migration through the release of ALK-bound β-catenin, leading to its nuclear localization and subsequent activation of EMT gene expression.

The MMP-9 protease induces ALK ECD cleavage

Many receptor tyrosine kinases (RTKs) undergo ECD cleavage by proteases (sheddases), which include matrix metalloproteinases (MMPs) and a disintegrin and metalloproteinases (ADAMs) (Kreitman et al., 2018). These zinc-dependent, membrane-associated or secreted proteases cleave cell surface transmembrane proteins that have primary roles in extracellular matrix protein degradation. To identify the candidate protease(s) that mediate cleavage, we first investigated ADAM family members implicated in RTK cleavage, including ADAMs 10 and 17, which induce cleavage of AXL, MET, and ErbB4 (O'Bryan et al., 1995; Rio et al., 2000; Schelter et al., 2010). Short hairpin RNA (shRNA)-mediated knockdown of these proteases in NB cells expressing WT cleavable ALK did not affect ALK cleavage (Figure S7A), leading us to next test the effects of MMP inhibition. The broad-spectrum protease inhibitors GM6001 (affecting MMP-1, MMP-2, MMP-3, MMP-8, and MMP-9) and CAS 204140–01-2 (MMP-9 and MMP-13) caused a decrease in the shed ALK ECD fragment (Figure 7A), whereas MMP408 (MMP-3, MMP-12, and MMP-13 but not MMP-9) (Li et al., 2009) did not affect cleavage (Figure 7B). The selective MMP-9 inhibitor CTK8G1150 (MMP-9, MMP-1, and MMP-13) (Levin et al., 2001), however, produced a marked decrease in the shed fragment, thereby narrowing the candidate protease to MMP-9 (Figure 7B). These results were further substantiated by *in silico* protease substrate analysis that predicted the ALK cleavage site to contain the consensus substrate sequence for MMP-9 (Figure S7B) (Song et al., 2012). CTK8G1150 treatment also led to significant inhibition of ECD cleavage in 293T and NIH 3T3 cells engineered to overexpress WT ALK, with a commensurate decrease in the shed fragment (Figure S7C). ALK ECD cleavage was disrupted in a dose-dependent manner and was maintained over a relatively prolonged period (>52 h) (Figures S7D and S7E). Importantly, the same compound also inhibited ECD cleavage in multiple WT ALK-expressing NB cell lines (Figure 7C). Genetic depletion of MMP-9 through shRNA knockdown in two NB cell lines (NGP and BE(2)-C) revealed a significant decrease in the 140-kDa cleavage product, indicating inhibition of cleavage (Figure 7D). Depletion of

MMP-2, by contrast, led to only a slight decrease in cleavage (data not shown). Additionally, treatment of purified WT ALK, but not the ALK LF655del protein with recombinant human MMP-9-induced cleavage (Figure S7F), pointed to the role of this MMP as an ALK sheddase. Finally, treatment with the MMP-9 inhibitor significantly suppressed the migration of NB cells that endogenously express WT ALK (Figure 7E). Together, these results identify MMP-9 as the mediator of ALK ECD cleavage, whose effect on NB cell migration can be abolished by treatment with a specific MMP-9 inhibitor.

DISCUSSION

Ectodomain cleavage is a feature of many transmembrane RTKs, in which shedding leads to activation or repression of the receptor (Kreitman et al., 2018). In breast cancer, ECD cleavage of the HER2 receptor generates membrane-bound p95-HER2, which imparts growth and survival signals to the cell (Liu et al., 2006). By inhibiting such cleavage, the anti-HER2 antibody trastuzumab disrupts HER2 signaling and blocks cell cycle progression, improving patient outcome (Molina et al., 2001). Similarly, the AXL receptor, whose upregulation arises as a mechanism of resistance to various kinase inhibitors, including ALK in NB (Debruyne et al., 2016; Zhang et al., 2012), also undergoes ECD cleavage; however, this process in certain cells represses AXL and slows tumorigenesis (Miller et al., 2016). Here, we show that ALK undergoes ECD cleavage at Asn654-Leu655, mediated by the MMP-9 matrix metalloprotease, and thereby promotes the migration and invasion of NB cells.

We demonstrate that inhibition of ECD cleavage in NB cells that endogenously express ALK leads to the suppression of cell migration and invasion, which can be rescued by overexpression of WT-cleavable ALK. Importantly, exogenous expression of the WT-cleavable receptor in both NB and non-NB cells that express minimal or no ALK results in significantly increased cell migration, an effect that was not noted with the cleavage-site mutant proteins. These observations suggest a prominent role for ECD shedding of the ALK receptor in cell migration, which is also reflected in the enrichment of transcripts involved in neuronal migration in cleavage-inhibited NB cells. Downregulation of EMT signatures and the differential expression of critical proteins that regulate cell migration are consistent with the failure of those cells to metastasize *in vivo*. ALK ECD cleavage also occurs in early postnatal mouse brain cells. During development, activation of an EMT program is essential for the migration of cells that form the neural crest, enabling their dispersion to multiple sites throughout the body, including sympathetic ganglia (Thiery et al., 2009). Together with the highly conserved ALK cleavage site across different mammalian species, these observations suggest that ECD shedding is critical for neural crest cells to undergo EMT and migrate during development, and when aberrantly expressed in NB cells, potentiating tumor cell invasion and metastasis. The recent finding of structural genomic alterations that result in deletion of the ALK N-terminal domain in 2.4% of primary patient samples (Brady et al., 2020) reinforces the functional relevance of this phenomenon.

Whether the increased cell migration after ALK ECD cleavage is regulated by the truncated membrane-bound receptor that remains after ECD shedding or the shed ECD is not entirely clear because exposure to either fragment failed to affect cell migration. Alternatively, the

retention of β-catenin bound to cleavage-inhibited ALK, with subsequently lower nuclear β-catenin and its decreased occupancy at key EMT gene promoters offer a potential link between ALK ECD cleavage and EMT. Full-length ALK binds to β-catenin (Alshareef et al., 2016, 2017) (and this study), and therefore, we surmise that shedding of the ECD fragment disrupts the interaction between membrane-bound, truncated ALK and β-catenin, leading to the release of β-catenin and enabling its nuclear translocation and transcription of genes involved in cell migration. β-catenin also undergoes nuclear translocation in neural crest cells during development, where it activates SNAIL and SLUG EMT gene transcription, which, in turn, repress E-cadherin expression (Barrallo-Gimeno and Nieto, 2005; Shoval et al., 2007). Whether ALK cleavage contributes to neural crest cell migration requires further study. ALK ECD shedding could also be a prerequisite for subsequent intracellular cleavage as described for other heavily glycosylated proteins, such as trophoblast cell-surface antigen 2 (Trop2) and epithelial cell adhesion molecule (EpCAM) (Maetzel et al., 2009; Stoyanova et al., 2012). Indeed, caspase-dependent cleavage at the juxta-membrane intracytoplasmic region of the ALK receptor has been shown to cause anti- or pro-apoptotic effects depending on the presence or absence of ligand, respectively (Mourali et al., 2006). Thus, further elucidation of the subsequent proteolytic events of the ALK receptor is necessary to understand its role in tumorigenesis and during development.

ALK ectodomain shedding did not affect its phosphorylation at Y1507 and Y1604, and it did not appear to affect its kinase activity. One possible explanation for these findings is that ectodomain cleavage does not remove the ligand binding region, so that the receptor can still be activated through ligand binding. It is also possible that kinase domain activation of ALK and subsequent growth-promoting properties are separate from its role in EMT regulation as reflected by the lack of effect on cell growth and downstream signaling with ECD cleavage inhibition. However, downstream signaling was decreased in NIH 3T3 cells expressing ALK cleavage-site mutations. Possible reasons for this discrepancy include the not-insubstantial contribution of other dominant oncogenic stimuli in NB cells, such as MYCN amplification or the maintenance of signaling through compensatory mechanisms.

The preponderance of evidence in this study identified MMP-9 as the protease that cleaves the ALK ECD. However, we do not rule out the possibility that the ECD can be cleaved by other proteases, such as MMP-2 (Song et al., 2012). MMP-9, together with MMP-2, is involved in extracellular matrix remodeling during many biological processes, including invasion, neurite growth, and embryonic development (Vandooren et al., 2013). Activation of extracellular MMP-9 activity triggers cell motility, not only because of cleavage of its target molecules within the plasma membrane or extracellular matrix (such as cell adhesion molecules) but also because MMP-9 can efficiently degrade the extracellular matrix, an important prerequisite for metastasis (Tanjore and Kalluri, 2006). Moreover, MMP-9 has been shown to cooperate with SNAIL to potentiate cell migration (Lin et al., 2011), and SNAIL, in turn, positively regulates MMP-9 expression (Jordà et al., 2005). Schwannian-stroma-rich NBs are characteristically non-metastatic, and incubation of NB cells in Schwann cell media abolishes ALK cleavage (Degoutin et al., 2009), likely because of the production of natural MMP-9 inhibitors by Schwann cells, such as tissue inhibitors of metalloproteinase, TIMP-1 and TIMP-2 (Brew and Nagase, 2010; Huang et al., 2000; Kim et al., 2012). The selective MMP-9 antibody (andeca-liximab; Gilead, GS-5745) achieved

target engagement without dose-limiting toxicity and showed encouraging activity when combined with standard chemotherapy in patients with gastric and gastroesophageal junction adenocarcinoma (Shah et al., 2018) and may be a therapeutic strategy that could be tested in patients with NB.

In conclusion, the discovery of activating mutations in the ALK receptor more than a decade ago has led to numerous studies to understand the effect of aberrant ALK signaling on NB pathobiology and to devise clinically effective countermeasures. These efforts have yielded a series of ALK inhibitors with the ability to silence oncogenic ALK expression and to block the growth of NB cells in experimental models (Hallberg and Palmer, 2016), but to date, this progress has not translated to clear therapeutic gains (Foster et al., 2021). Although newer generations of inhibitors may be more effective, success with direct targeting of ALK kinase activity would benefit only the approximately 10% of high-risk patients with NB who have tumors harboring activating mutations, leading to efforts to harness ALK as a tumor-associated antigen. Here, we show that proteolytic cleavage of the ECD of WT ALK, which is expressed in most NB cases promotes metastasis and that by targeting that process, these adverse cancer-associated features of ALK cleavage can be circumvented, raising the possibility of MMP-9 inhibition, either singly or in combination with that of ALK in patients with NB. The identification of the cleavage site in both ALK WT and mutated cells has additional implications for immunotherapies based on expression of the full-length receptor on the cell surface because antibodies and/or other strategies specific to epitopes in the shed ECD would not be able to bind to the truncated membrane-bound receptor. Blockade of ECD shedding by co-treatment with an MMP9 inhibitor could be used as a strategy to increase the available expression of full-length ALK on the cell surface, thereby also enabling NK cell effector activity. The shed ALK ECD also could be used as a biomarker to non-invasively and longitudinally monitor disease activity in patients with NB. Finally, it will be important to determine whether ALK ECD cleavage also occurs in the other cancers in which the full-length receptor is expressed and whether its effects recapitulate our findings in NB.

STAR★METHODS

KEY RESOURCES TABLE

REAGENT or RESOURCE	SOURCE	IDENTIFIER
Antibodies		
Rabbit monoclonal anti-GAPDH	Cell Signaling Technology	Cat#2118; RRID: AB_561053
Mouse monoclonal anti-ALK (4C5B8)	Life Technologies	Cat#354300; RRID: AB_2533203
Rabbit monoclonal anti-ALK (C26G7)	Cell Signaling Technology	Cat#3333; RRID: AB_836862
Rabbit polyclonal anti-Phospho-ALK (Tyr1507)	Abcam	Cat#ab73996; RRID: AB_2226754
Rabbit monoclonal anti-Phospho-ALK (Tyr1604)	Cell Signaling Technology	Cat#3341; RRID: AB_331047
Rabbit monoclonal anti-E-Cadherin (24E10)	Cell Signaling Technology	Cat#3195; RRID: AB_2291471
Rabbit Polyclonal anti-β-Actin	Cell Signaling Technology	Cat#4967; RRID: AB_330288

REAGENT or RESOURCE	SOURCE	IDENTIFIER
Rabbit monoclonal anti-p44/42 MAPK	Cell Signaling Technology	Cat#4695; RRID: AB_390779
Rabbit monoclonal anti-Phospho-p44/42 MAPK(Thr202/Tyr204)	Cell Signaling Technology	Cat#4377; RRID: AB_331775
Rabbit monoclonal anti-Stat3	Cell Signaling Technology	Cat#4904; RRID: AB_331269
Rabbit Polyclonal anti-Phospho-Stat3(Tyr705)	Cell Signaling Technology	Cat#9131; RRID: AB_331586
Rabbit monoclonal anti-Akt	Cell Signaling Technology	Cat#4691; RRID: AB_915783
Rabbit Polyclonal anti-Phospho-Akt (Ser473)	Cell Signaling Technology	Cat#9271; RRID: AB_329825
Rabbit Polyclonal anti-Phospho-Akt (Thr308)	Cell Signaling Technology	Cat#9275; RRID: AB_329828
Mouse monoclonal anti-ALK (F-12)	Santa Cruz Biotechnology	sc-398791; RRID: AB_2889357
Rabbit monoclonal anti-Snail	Cell Signaling Technology	Cat# 3879; RRID: AB_2255011
Rabbit monoclonal anti-Slug	Cell Signaling Technology	Cat# 9585; RRID: AB_2239535
Rabbit monoclonal anti-N-Cadherin	Cell Signaling Technology	Cat#13116; RRID: AB_2687616
Rabbit monoclonal anti-MMP-9	Cell Signaling Technology	Cat#13667; RRID: AB_2798289
Rabbit monoclonal anti-HA-Tag (C29F4)	Cell Signaling Technology	Cat# 3724; RRID: AB_1549585
Rabbit monoclonal anti-DYKDDDDK Tag(D6W5B)	Cell Signaling Technology	Cat#14793; RRID: AB_2572291
Mouse monoclonal anti-ADAM10	Abcam	Cat#ab73402; RRID: AB_10562808
Mouse monoclonal anti-ADAM17	Abcam	Cat#ab57484; RRID: AB_940131
Rabbit monoclonal anti-β-Catenin (D10A8)	Cell Signaling Technology	Cat# 8480; RRID: AB_11127855
Goat anti-Rabbit IgG (H+L) Secondary Antibody, Biotin Conjugate	Thermo Fisher	Cat#65–6140; RRID: AB_2533969
Alexa Fluor 568 Donkey Anti-Mouse IgG	Thermo Fisher	Cat#A10037; RRID: AB_2534013
Mouse monoclonal anti-ALK 8G7	This paper	N/A
Bacterial and virus strains		
DH5α *E. coli*	Thermo Fisher	Cat# 18265017
Stbl3 *E. coli*	Life Technologies	Cat# C7373–03
Biological samples		
Patient-derived xenografts (PDX) tumor tissue	St. Jude Children's Research Hospital (CRH)	SJNBL046148_X1
Patient-derived xenografts (PDX) tumor tissue	St. Jude Children's Research Hospital	SJNBL013761_1
Chemicals, peptides, and recombinant proteins		
Full-length recombinant human MMP-9	Biolegend	Cat# 551102
CTK8G1150	Millipore	Cat#444278; CAS 1177749–58-4
CAS 204140–01-2	Millipore	Cat# 444252
GM6001	Enzo Life Sciences	Cat# 89158–002
MMP408	Millipore	Cat#444291; CAS 1258003–93-8
Streptavidin-TXRD	SouthernBiotech	Cat#7100–07; RRID: AB_2533969

REAGENT or RESOURCE	SOURCE	IDENTIFIER
Critical commercial assays		
CellTiter-Glo Luminescent Cell Viability Assay	Promega	Cat# G7573
SuperScript III Reverse Transcriptase	Thermo Fisher	Cat# 18080044
QIAamp DNA mini Kit	QIAGEN	Cat# 51304
QCM ECMatrix Cell Invasion Assay	MilliporeSigma	Cat# ECM554
24-Well Translucent Cell Culture Inserts	Falcon	Cat# 353097
FLAG® M Purification Kit -For Mammalian expression systems	Sigma-Aldrich	Cat# CELLMM2
Lipofectamine 3000	Life Technologies	Cat# L3000015
QuikChange XL II Site-Directed Mutagenesis Kit	Agilent Technologies	Cat# 200522
Pierce Cell surface protein isolation kit	Thermo Scientific	Cat# 89881
mirVana miRNA Isolation Kit	Life Technologies	Cat# AM1561
QuantiFast SYBR Green PCR kit	QIAGEN	Cat# 204057
Universal Tyrosine Kinase Assay Kit	Takara	Cat# MK410
DC protein assay kit	Bio-Rad	Cat# 500–0111
Deposited data		
Microarray data	This paper	GEO: GSE140025
Experimental models: Cell lines		
Human: HEK293T	ATCC	CRL-3216
Human: NGP:	Children’s Oncology Group	N/A
Human: Kelly:	Children’s Oncology Group	N/A
Human: IMR-5:	Children’s Oncology Group	N/A
Human: BE(2)-C:	ATCC	CRL-2268
Human: NBL-S	Children’s Oncology Group	N/A
Human: SH-SY5Y	Children’s Oncology Group	CRL-226
Mouse: NIH 3T3	ATCC	CRL-1658
Human: SK-N-AS	Children’s Oncology Group	N/A
Human: CHP-212	ATCC	CRL-2273
Experimental Models: Organisms/Strains		
Mouse: C57BL/6J	The Jackson Laboratory	JAX: 000664
Mouse: NOD/SCID	UHN (University Health Network)	N/A
Oligonucleotides		
Primers and Oligonucleotides see Table S1.		
Recombinant DNA		
pcDNA3.1-ALK-HA	This paper	N/A

REAGENT or RESOURCE	SOURCE	IDENTIFIER
pcDNA3.1-ALK LF655del –HA	This paper	N/A
pTT-FAM150A-HA	Guan et al., 2015	N/A
pcDNA3-FAM150B-HA	Guan et al., 2015	N/A
TGL reporter	Ponomarev et al., 2004	N/A
pSpCas9(BB)-2A-Puro (PX459) V2	Ran et al., 2013	Addgene plasmid: Cat# 62988; RRID: Addgene_62988
PX459-ALK-gRNA	This paper	N/A
pLKO.1-puro eGFP shRNA Control Plasmid	Sigma	Cat# SHC005
MSCV-ALK	This paper	N/A
MSCV-ALK LF655del	This paper	N/A
MSCV-ALK 655–1604	This paper	N/A
MSCV-ALK Δ1–654	This paper	N/A
MSCV-ALK p140	This paper	N/A
MSCV-ALK D636–682	This paper	N/A
MSCV-FLAG-ALK	This paper	N/A
MSCV-FLAG-ALK LF655del	This paper	N/A
MSCV-ALK F656D	This paper	N/A
MSCV-LF655RD	This paper	N/A
MSCV-LF655FY	This paper	N/A
MSCV-NLF655KRD	This paper	N/A
MSCV-ALK KSRNLF651del	This paper	N/A
MSCV-ALK KSRNLFER651del	This paper	N/A
MSCV-ALK ECD del	This paper	N/A
pcDNA3.1-ALK	This paper	N/A
pcDNA3.1-ALK L655K	This paper	N/A
Software and algorithms		
GraphPad Prism 7.0 and 8.0	GraphPad	https://www.graphpad.com/scientific-software/prism/
PANTHER Classification System	PANTHER Classification System	http://pantherdb.org/:
GSEA	Broad Institute	https://www.gsea-msigdb.org/gsea/index.jsp
Scaffold	Proteome Software, Inc	http://www.proteomesoftware.com/products/scaffold-5
ImageJ	Schneider et al., 2012	https://imagej.nih.gov/ij/download.html
PROSPER	Monash University;: Song et al., 2012	https://research.monash.edu/en/publications/prosper-an-integratedfeature-based-tool-for-predicting-protease-
FlowJo	FlowJo LLC	https://www.flowjo.com/

RESOURCE AVAILABILITY

Lead contact—Further information and requests for reagents and resources should be directed to and will be fulfilled by the lead contact, Rani E. George (rani_george@dfci.harvard.edu)

Materials availability—All unique/stable reagents generated in this study are available from the Lead Contact with a completed Materials Transfer Agreement.

Date and code availability—Microarray data can be found in the NCBI Gene Expression Omnibus under the accession code GSE140025. This paper does not report original code. Any additional information required to reanalyze the data reported in this paper is available from the lead contact upon request.

EXPERIMENTAL MODEL AND SUBJECT DETAILS

Cell lines—Human neuroblastoma (NB) cell lines (NGP, IMR5, Kelly, NBL-S, SH-SY5Y, SK-N-AS, CHP-212) were obtained from the Children's Oncology Group cell line bank under an MTA. The BE (2)-C, NIH 3T3 and HEK293T cells were purchased from the American Type Culture Collection (ATCC). Cell lines were authenticated by genotyping at the DFCI Core Facility. NB cell lines were grown in RPMI-1640 medium supplemented with 10% fetal bovine serum (FBS) and 1% penicillin/streptomycin (Invitrogen). HEK293T cells were grown in DMEM medium supplemented with 10% FBS and 1% penicillin/streptomycin. NIH 3T3 cells were grown in DMEM with 10% fetal calf serum (FCS; Sigma-Aldrich) and 1% penicillin/streptomycin. Cells were cultured at 37°C in 5% CO_2. Cell lines from male subjects: NGP, BE (2)-C, IMR5, NBL-S, CHP-212, NIH 3T3. Cell lines from female subjects: Kelly, SH-SY5Y, SK-N-AS, HEK293T.

Mouse models—For the metastasis study, animal experiments were performed on an approved Toronto SickKids Institutional protocol. 9-week-old NOD/SCID female mice obtained from the University Health Network Immune-deficient Mouse Colony (Toronto) were used in the intracardiac injection model. For the tail vein injection model, 6–8-week-old NOD/SCID female mice obtained from the University Health Network Immune-deficient Mouse Colony (Toronto) were used. Animals were monitored for health, weight, appearance, and metastatic burden and sacrificed following the SickKids Institutional Animal Utilization Protocol. For collection of tissue samples, all mouse experiments were performed with approval from the Institutional Animal Care and Use Committee (IACUC) of the DFCI. Neuroblastoma patient-derived xenografts (PDX) were received from St. Jude Children's Research Hospital and expanded in female nude mice (Crl:NU-Foxn1nu) obtained from Charles River Laboratory. Mice brain tissues were collected from female C57BL/6J mice.

METHODS DETAILS

Western blotting—Cell lysates were prepared in NP-40 buffer (Invitrogen) containing complete protease inhibitor (Roche), phosphatase inhibitor (Roche) and phenylmethylsulfonyl fluoride (PMSF). Lysates were incubated on ice for 20 min and centrifuged at 16,000 g for 15 min at 4°C. Protein concentrations of the supernatants were

determined with the DC protein assay kit (Bio-Rad). Protein samples were denatured using NuPAGE LDS sample buffer (Invitrogen) and NuPAGE sample reducing agent (Invitrogen). Proteins were then separated on precast 4%–12% Bis-Tris gels (Invitrogen) and transferred to nitrocellulose membranes (Bio-Rad). After blocking in blocking buffer (5% dry milk in TBS with 0.2% Tween-20), membranes were incubated with the primary antibody overnight at 4°C, washed three times with TBST buffer, chemiluminescent detection performed with the appropriate secondary antibodies and developed using Genemate Blue ultra-autoradiography film (VWR).

Mass spectrometry (MS) sample preparation—NGP cells were grown in serum-free RPMI-1640 medium for 72 hours. Conditioned medium was collected and concentrated (more than 40X) using an ultra-15 centrifugal filter (Amicon) at 4°C. The concentrated medium was then subjected to co-immunoprecipitation (co-IP) using the N-terminal 8G7 ALK antibody. Proteins were separated on SDS-PAGE gels (Thermo Fisher Scientific; 4%–12% Bio-Tris gel) before staining with Coomassie Blue R-250 (Bio-Rad). The band corresponding to the ALK ectodomain was excised, sequentially washed with 50% methanol/water and 47.5/47.5/5% methanol/water/acetic acid, dehydrated with acetonitrile, reduced with DTT and alkylated with iodoacetamide. The sample was then sequentially washed with 50 mM ammonium bicarbonate/50% acetonitrile and acetonitrile, and enzymatically digested with trypsin or chymotrypsin. The digested sample was injected onto a C18 trap column and eluted onto an analytical column (Jupiter C18 column, Phenomenex). The digested extracts were analyzed by reversed-phase high-performance liquid chromatography (HPLC) (C18 column) and Tandem MS using an Orbitrap Elite mass spectrometer (Thermo Fisher Scientific). Peptides were identified from the MS data using SEQUEST algorithms. A species-specific database generated from the NCBI non-redundant database (nr.fasta) was used to identify the peptides. The resulting data were then loaded onto Scaffold (Proteome Software, Portland, OR) for analysis. A peptide threshold of 95% was used for identification of peptides.

Site-directed mutagenesis—Site-directed mutagenesis was performed using a PCR-based strategy. Point mutations within the plasmid construct were introduced by site-directed mutagenesis using the QuikChange II Site-Directed Mutagenesis Kit (Agilent Technologies) following the manufacturer’s instructions. The resulting mutant plasmids were verified by DNA sequencing. ALK 655–1604 was generated using the Q5 site Mutagenesis Kit (NEB) following the manufacturer’s instructions.

Stable cell line preparation—The retrovirus was packaged by cotransfection of pLKO.1 shRNA construct and the helper plasmids pMD.MLV and pMD2.G-VSV-G into HEK293T cells using TransIT-LT1 Transfection Reagent (Mirus). The virus-containing supernatant was harvested and filtered through a 0.45 μm polyvinylidene fluoride (PVDF) filter (VWR) and applied to cells in the presence of polybrene (10 μg/ml). After 48 hours, cells were selected with puromycin (NIH 3T3 cells 2 μg/ml; NGP cells 2.5 μg/ml; SK-N-AS cells 2 μg/ml; CHP-212 cells 1 μg/ml; 293T cells 2 μg/ml) or fluorescence-activated cell sorting (FACS).

Cell surface protein analysis—Cell surface protein isolation was conducted using a cell-surface protein isolation kit (Pierce) according to the manufacturer's instructions with minor modifications. Biotinylated proteins were isolated with neutravidin agarose resin (Thermo Scientific) which was packed in an isolation column. After the biotinylated proteins were eluted with the SDS-containing sample buffer, proteins were analyzed by SDS-PAGE and western blotting.

Glycosylation assay—The Peptide N-Glycosidase F (PNGase F) deglycosylation assay (New England Biolabs) was performed according to the manufacturer's instructions. Cell lysates from $NGP^{CRISPR\ ctrl}$ or $NGP^{ALK(LF655del)}$ cells prepared with NP-40 buffer were denatured at 100°C for 10 minutes in the presence of glycoprotein denaturing buffer and incubated with PNGase F in GlycoBuffer (1X) at 37°C for 1hr, following which ALK deglycosylation was analyzed through immunoblotting with anti-ALK antibodies.

FLAG fusion protein purification—The MSCV-FLAG-ALK or MSCV-FLAG-ALK LF655del expression constructs were transiently transfected into 293T cells using TransIT-Express Transfection Reagent (Mirus) to express ALK proteins. Recombinant wild-type ALK or mutant ALK proteins were purified using an anti-FLAG purification kit (Sigma-Aldrich) according to the manufacturer's instructions. The affinity purification was performed using an anti-Flag M2 affinity gel, a highly specific monoclonal antibody covalently attached to agarose resin.

Co-immunoprecipitation (Co-IP)—HEK293T cells were transiently transfected with WT and mutant ALK constructs to express HA-tagged and FLAG-tagged proteins. Cells were washed with PBS and harvested in IP lysis buffer (50 mM Tris-HCL buffer (pH 7.4), 100 mM NaCl, 1% Triton-100, 1 mM PMSF), containing the cocktail protease inhibitor (Roche) and phosphatase inhibitor (Roche). Homogenates were centrifuged at 20,000 g for 10 min at 4°C. Supernatants were collected and co-IP performed using Dynabeads protein G (Life Technologies) according to the manufacturer's instructions. Briefly, Dynabeads were incubated with either anti-FLAG or anti-HA antibody, washed to remove unbound primary antibody, and incubated with cell lysates for immunoprecipitation of the target antigen. The elution step was performed by heating the beads for 10 min at 95°C in premixed NuPAGE LDS sample buffer and NuPAGE sample reducing reagent (Invitrogen). Samples were then loaded onto NuPAGE 4%–12% Bis-Tris protein gels (Invitrogen), proteins transferred to nitrocellulose membranes (Bio-Rad) and immunoblotting performed as described above.

***In vitro* kinase assay—**The Universal Tyrosine Kinase Assay kit (Takara) was used to measure kinase activity according to the manufacturer's instructions. Briefly, NIH 3T3 cells stably expressing WT ALK or ALK CSMs were harvested in extraction buffer, lysates incubated on ice for 20 min, centrifuged at 10,000 g for 10 min at 4°C and the supernatants pre-cleared with 50 μL protein G agarose beads for 30 min at 4°C under rotation. 10 μL ALK antibody was then added to the supernatant and incubated at 4°C under rotation for 4 hr. 30 μL protein G agarose beads were then added to the supernatant and incubated at 4°C under rotation for 2 hr. The immunoprecipitated material was then washed with PBS and used in the kinase assay.

Preparation of ALK ligand-conditioned medium—HEK293 cells were grown in 10 cm dishes to 90% confluency and transfected with 10 μg each of the following plasmids: pcDNA3 vector control, pTT5-FAM150A-HA or pcDNA3-FAM150B-HA with lipofectamine 3000 following the manufacturer's instructions (Invitrogen). After 12 hr., the medium was replaced with serum-free medium. After 24 hr. incubation at 37°C in 5% CO_2, the conditioned medium was harvested for the experiment. 1 mL of harvested medium (control, ALKAL1- or ALKAL2-conditioned) was added to 6-well plates of NIH 3T3 cells stably expressing WT or mutant ALK, incubated for 1 hr. at 37°C in 5% CO_2, harvested and used in WB analysis of ALK and mutant ALK activation.

Expression of human ALK mutants in the *Drosophila* eye—The Gal4-UAS system was applied to ectopically express human ALK constructs within the *Drosophila* eye. *Drosophila* stocks w^{1118} and *GMR-Gal4* (stock number 5905 and 9146, respectively) from Bloomington *Drosophila* Stock Center (Indiana University) were used. Generation of the *Drosophila* transgenic *UAS-ALK* and *UAS-ALKAL2(FAM150A)* lines were described previously (Guan et al., 2015; Schönherr et al., 2012). *UAS-ALK LF655del* was synthesized (GenScript). Transgenic flies were obtained by injection (BestGene Inc.). Transgenic *Drosophila* lines carrying the *UAS-ALK*, *UAS-ALKAL2, UAS-ALK LF655del or UAS-*ALK^{F1174L} were crossed with the *GMR-Gal4* transgenic driver line to drive ectopic expression of the ALK variants in the eye imaginal discs. Experiments were conducted at 25°C. Adult flies were collected and frozen at −25°C prior to microscopic analysis with a Zeiss AxioZoomV16 stereomicroscope.

CRISPR-Cas9-mediated gene editing—Genomic editing experiments were conducted using CRISPR-Cas9 editing as previously described (Ran et al., 2013). A single guide RNA (sgRNA) was designed using the GPP sgRNA Designer Tool (Broad Institute). An ALK-single stranded oligonucleotide (ssODN), purchased from Integrated DNA Technologies (IDT), was used to introduce precise genomic editing through homology-directed repair (HDR). The guide RNA was first cloned into the BbsI site of the pSpCas9(BB)-2A-Puro (PX459) V2.0 vector (Addgene) to generate plasmid PX459-ALK-gRNA. NGP cells were then transiently transfected with this plasmid and ALK-ssODNs using Lipofectamine 3000 (Thermo Fisher Scientific). Cells were incubated at 37°C for 30 hr., selected for 48 hours in 2.5 μg/ml puromycin, expanded, and diluted to single cells into 96-well plates. Single-cell clones were identified and allowed to expand for 6 weeks, following which cell editing was validated by sequencing. gRNA and ssODN sequences available on request.

Immunofluorescence analysis—Cells (0.5×10^6 per well) were seeded into six-well plates and grown on glass coverslips for 24 hr. before fixation in 4% paraformaldehyde in PBS for 15 min at room temperature (RT), washed with PBS, permeabilized in 0.1% Triton X-100, and blocked with PBS containing 0.05% Tween-20 and 5% BSA for 1 hr. to block nonspecific binding. Then, cells were incubated with the 8G7 antibody (1:100) overnight at 4°C. After washing with PBS, cells were incubated with AlexaFluor 568-conjugated secondary antibody for 1 hr. at 25°C. Images were collected on a Zeiss AXIO Imager Z1 fluorescence microscope. For β-catenin immunofluorescence measurement, cells were plated onto poly-lysine coated coverslips in a 12-well plate. After 24 hours, cells were

washed once in PBS, fixed in 4% paraformaldehyde in PBS, washed, permeabilized in 0.1% Triton X-100, and blocked in PBS containing 10% horse serum. Cells were incubated in β-catenin primary antibody (1:500) overnight. The next day, cells were washed, incubated in goat anti-rabbit IgG secondary antibody (1:1000) for 1 hr. washed, and incubated in Streptavidin-TexasRed (1:1000) for 1 hr. Coverslips were mounted onto slides using mounting medium containing DAPI. Images were collected on a Zeiss AXIO Imager Z1 fluorescence microscope.

Cell growth assay—Cells (1×10^3 per well) were plated in 96-well plates on day 0 and analyzed for growth at intervals using the CellTiter-Glo Luminescent Cell Viability Assay (Promega) according to the manufacturer's instructions. The results were collected using the FLUOstar Omega microplate reader (BMG Labtech) and analyzed using MARS software (BMG Labtech).

Focus formation assay—Cells (1×10^3 per well) were seeded into 6-well plates, incubated at 37°C in 5% CO_2 for 14 days, with media replaced every 4 days. After 14 days, the medium was removed, cells were fixed with 100% methanol and stained with 0.5% crystal violet for 20 min at room temperature, rinsed with ddH_2O and focus formation analyzed by eye after air-drying.

Soft agar colony formation—For soft agar assays, experiments were carried out in 24 well plates coated with a base layer of RPMI containing 0.5% agar, and 10% FBS. Cells (5×10^3 per well) were seeded in RPMI containing 0.35% agarose, and 10% FBS and incubated for 14 days during which 0.5 mL fresh medium was added to each well every 5 days. After incubation for 14 days at 37°C in 5% CO_2, plates were subjected to 0.005% crystal violet staining for 2 hr. Colony formation was analyzed using an IX70 inverted optical microscope (Olympus).

RNA extraction and gene expression analysis—$NGP^{CRISPR\ ctrl}$ or $NGP^{ALK(LF655del)}$ cells (8×10^6 cells per replicate) were collected and total RNA extracted using TRIzol Reagent followed by purification using the mirVana miRNA Isolation Kit (Thermo Scientific) according to the manufacturer's instructions. The quality of all RNA samples was checked using NanoDrop 2000 (Thermo Scientific). RNA samples were spiked-in with ERCC RNA Spike-In Mix (Ambion) for expression normalization. PrimeView Human Gene Expression Array GeneChip (Affymetrix) was used for the gene expression assays. Preparation of cDNA, hybridization, and scanning of microarrays were performed at the DFCI core facility according to the manufacturer's protocols (Affymetrix).

Microarray data analysis—Microarray data were analyzed using a custom CDF file (GPL16043) that contained the mapping information of the ERCC probes used in the spike-in RNAs. The arrays were normalized as previously described (Lovén et al., 2012). In brief, all microarray chip data were imported in R (https://www.r-project.org/, v.3.5.1) using the affy package (v.1.44.0) (Gautier et al., 2004), converted into expression values using the expresso command, normalized to take into account the different numbers of cells and spike-ins used and renormalized using loess regression fitted to the spike-in probes. Sets of differentially expressed genes were obtained using the limma package (v.3.22.7) (Smyth et

al., 2003) and an FDR value of 0.05. Gene set enrichment analysis (GSEA) was performed using GSEA v3.0 software (Broad Institute). Significantly enriched gene sets were evaluated as per standard criteria (FDR ≤ 0.25 and nominal P value ≤ 0.05). Gene ontology analysis was performed using the PANTHER classification system.

Quantitative RT-PCR—Total RNA was extracted from cells (8×10^6 cells per replicate) using TRIzol Reagent followed by purification using the mirVana miRNA Isolation Kit (Thermo Scientific). cDNA was synthesized from 1 μg of purified RNA using SuperScript III reverse transcriptase system (Invitrogen) following the manufacturer's protocol. qPCR was performed using the QuantiFast SYBR Green PCR kit (QIAGEN) with a Biosystems ViiA 7 Real-Time PCR System (Life Technologies). The housekeeping gene GAPDH was used as an internal control to normalize the variability in expression levels. The ΔΔCt relative quantification method was performed to measure relative quantitation of mRNA.

Cell invasion assay—The QCM™ ECMatrix™ Cell Invasion Assay Kit (Millipore) was used with minor modifications. Cells were incubated in serum-free medium for 18 hr. at 37°C in 5% CO_2. A cell suspension containing 5×10^5 cells/mL in serum-free medium was added to the upper chamber. Serum-containing medium was added to the lower chamber. NGP and NIH 3T3 cells were incubated for 72 and 24 hr. respectively and the protocol followed as per the manufacturer's instructions.

Cell migration assay—Cell migration was measured using transwell chambers (Falcon; cell culture inserts with 8 μm pores) and a 24-well plate as the lower chamber. A cell suspension containing 0.5×10^6 cells/mL in serum-free medium was added to the upper chamber. Inserts were placed in the lower chamber containing medium with serum. NGP, NIH 3T3, CHP-212 and SK-N-AS cells were incubated at 37°C in 5% CO_2 for 48, 16, 24, and 8 hr. respectively. After incubation, cells remaining on the top surface of the insert were removed. Migrated cells were fixed with methanol, stained with crystal violet (Sigma-Aldrich), and photographed with a light microscope at 100X magnification.

Wound healing assay—Cells were seeded into 6-well plates to form a cell monolayer. When 70%–80% confluence was reached, the monolayer was scratched using a pipette tip. The scratched area at time point 0 hr. was set as the initial wound width. Cells were incubated in 5% $C0_2$ at 37°C, and the area not covered was measured at 24 to 48 hr. and photographed.

***In vivo* metastasis study—**NGP (NGP $^{\text{CRISPR ctrl}}$ or NGP $^{\text{ALK(LF655del)}}$) or SK-N-AS (SK-N-AS WT ALK cells or SK-N-AS ALK LF655del) neuroblastoma cells were infected with the retroviral TGL (thymidine kinase-GFP-luciferase) reporter to generate stable cell lines (Ponomarev et al., 2004). GFP-positive cells were selected through FACS. Luciferase activity of sorted cells was confirmed using the Luciferase Assay System (Promega). 1×10^5 cells were introduced into NOD/SCID mice via intracardiac injections as previously described (Kang et al., 2003; Seong et al., 2017). Animals were monitored for health, weight, appearance, and metastatic burden and sacrificed following the SickKids Institutional Animal Utilization Protocol. For imaging, mice were injected with D-luciferin (PerkinElmer) and imaged 10- and 12-minutes post-injection with the Xenogen IVIS

imaging system. Bioluminescence was quantified by drawing a region of interest (ROI) around each animal and measured as photon flux per second.

For the tail vein injection model, NOD/SCID mice were injected in the lateral tail vein with 5×10^5 cells in PBS. The animals were monitored and bioluminescence imaged. Endpoints were reached at whole body signal saturation and/or signs of morbidity.

Preparation of tissue samples—Mice brain tissues were collected from C57BL/6J mice and stored at −80°C after snap freezing in liquid nitrogen. Frozen PDXs and brain tissues were homogenized with electric homogenizer in cold NP-40 buffer (Invitrogen) containing complete protease inhibitor (Roche), phosphatase inhibitor (Roche), and PMSF. Lysates were incubated on ice for 20 min and centrifuged at 16,000 g for 15 min at 4°C. The supernatants were applied for western blotting.

ShRNA knockdown—pLKO.1 plasmid containing shRNA sequences targeting MMP-9 (sh#1: TRCN0000373008; sh#6: TRCN0000051438), ADAM10 (sh#1: TRCN0000006674; sh#3: TRCN0000006673), and ADAM17(sh#1: TRCN0000052171; sh#2: TRCN0000052170; sh#3: TRCN0000052172; sh#4: TRCN0000052168; sh#5: TRCN0000052169) were purchased from Sigma-Aldrich. pLKO.1 GFP shRNA was a gift from D. Sabatini, MIT (Addgene plasmid 30323). The lentivirus was packaged by co-transfection of the pLKO.1 shRNA, pCMV-dR8.91, and pMD2.G-VSV-G constructs into HEK293T cells using the TransIT-LT1 Transfection reagent (Mirus). The virus-containing supernatant was filtered with a 0.45 μm PVDF filter (VWR). Cells were then transduced with virus, followed by puromycin selection for two days.

***In vitro* cleavage assay—**Purified recombinant ALK or ALK LF655del proteins were incubated with recombinant human MMP-9 (Biolegend) in reaction buffer (50 mM Tris-HCl buffer, pH 7.4, 150 mM NaCl) containing 0.2 mM *p*-aminophenylmercuric acetate (Calbiochem) for 3 hr. at 37°C. The samples were then denatured using NuPAGE LDS sample buffer and NuPAGE sample reducing reagent (Invitrogen), loaded onto SDS-PAGE (4%–12% Bio-Tris) gels and WB performed as described above.

Chromatin immunoprecipitation-quantitative PCR (ChIP-qPCR)—Approximately $10–12 \times 10^7$ $NGP^{CRISPR\ ctrl}$ or $NGP^{ALK(LF655del)}$ cells were crosslinked with 1% formaldehyde (Thermo Scientific) for 10 min at room temperature (RT) followed by quenching with 0.125 M glycine for 5 min. The cells were then washed twice in ice-cold 1× Phosphate Buffered Saline (PBS), and the cell pellet equivalent of 4×10^7 cells were flash frozen and stored at −80°C. Cross-linked cells were lysed in lysis buffer 1 (50 mM HEPES-KOH pH7.5, 140 mM NaCl, 1 mM EDTA, 10% glycerol, 0.5% NP40, 0.25% Triton X-100). The resultant nuclear pellet was washed once in lysis buffer 2 (10 mM Tris-HCl pH 8, 200 mM NaCl, 1 mM EDTA, 0.5 mM EGTA) and then resuspended in sonication buffer (50 mM HEPES-KOH pH 7.5, 140 mM NaCl, 1mM EDTA, 1mM EGTA, 1% Triton X-100, 0.1% sodium deoxycholate, 0.2% SDS). Chromatin was sheared using a Misonix 3000 sonicator (Misonix) and at the following settings: 9 cycles, each for 30 s on, followed by 1 min off, at a power of approximately 20 W. The lysates were then diluted with an equal amount of sonication buffer without SDS to reach a final concentration of 0.1% SDS, centrifuged at

4000 rpm for 15 min at 4°C, and supernatants containing soluble chromatin were collected. For each ChIP, the chromatin equivalent of 1×10^7 cells was used. 10 μl of Protein G Dynabeads per sample (Invitrogen) were blocked with 0.5% BSA (w/v) in 1× PBS and were incubated with the following antibodies overnight at 4°C: 0.36 μg of anti-β-catenin (Cell Signaling Technology 8480S) or 1 μg of TCF4 (Cell Signaling Technology 2569S). The sonicated lysates were then incubated overnight at 4°C with the antibody-bound magnetic beads, following which the beads were sequentially washed with low-salt buffer (50 mM HEPES-KOH (pH 7.5), 0.1% SDS, 1% Triton X-100, 0.1% sodium deoxycholate, 1 mM EGTA, 1 mM EDTA, 140 mM NaCl), high-salt buffer (50 mM HEPES-KOH (pH 7.5), 0.1% SDS, 1% Triton X-100, 0.1% sodium deoxycholate, 1 mM EGTA, 1 mM EDTA, 500 mM NaCl), LiCl buffer (20 mM Tris-HCl (pH 8), 0.5% NP-40, 0.5% sodium deoxycholate, 1 mM EDTA, 250 mM LiCl), and Tris-EDTA (TE) buffer. DNA was then eluted in elution buffer (50 mM Tris-HCl (pH 8.0), 10 mM EDTA, 1% SDS) by incubation at 65°C for 40 min accompanied by constant shaking at 1000 rpm. Magnetic beads were pelleted by high-speed centrifugation and supernatants containing the eluted fraction were reverse crosslinked overnight at 65°C in the presence of 300 mM NaCl. The following day, RNA and protein were digested using RNase A and proteinase K, respectively, and DNA was purified with phenol-chloroform extraction and ethanol precipitation. Purified ChIP DNA was dissolved in 50 μl of 1× TE buffer. Quantitative PCR was performed on a ViiA 7 Real-Time PCR system (Thermo Fisher Scientific) with 2 μl purified DNA, 1× PowerTrack SYBR Green PCR master mix (Thermo Fisher Scientific), and PCR primers (200 nM) against the genomic regions of interest. Each individual biological sample was amplified in technical duplicate. β-Catenin and TCF4 occupancies at target gene promoters (*FN1*, *PITX2*, and *COL3A1*) were calculated as fold-enrichment relative to a negative control region (*GAPDH* promoter lacking TCF4 binding sites) using the $2^{-\Delta\Delta Ct}$ quantification method. First, the Δ Ct for each primer set was calculated using the following formula: Δ Ct = ChIP-DNA replicate average – input replicate average. Next, the final Δ Ct (ΔΔ Ct) for each target primer ChIP-DNA was calculated using the following formula: ΔΔ Ct = Δ Ct target primer set - Δ Ct negative (*GAPDH*) primer set. Finally, fold-enrichment values at target genes were normalized to $NGP^{CRISPR\ ctrl}$ to quantify the relative changes in β-Catenin and TCF4 binding in $NGP^{ALK(LF655del)}$ cells.

Subcellular fractionation—Isolation of subcellular fraction was conducted with Nuclei EZ Prep Nuclei Isolation Kit (Sigma) following the manufacturer's instructions.

Fluorescence-activated cell sorting analysis—For cell cycle analysis, cells were trypsinized and fixed in ice-cold 70% ethanol overnight at −20°C. After washing with ice-cold phosphate-buffered saline (PBS), cells were then treated with 0.5 mg/ml RNase A (Sigma-Aldrich) in combination with 50 μg/ml propidium iodide (PI, BD Biosciences). All FACS samples were analyzed on a FACSCanto II cell analyzer (Becton Dickinson) using Cell Quest software (Becton Dickinson). A minimum of 50,000 events were counted per sample and used for further analysis. Data were analyzed using FlowJo v10 software.

QUANTIFICATION AND STATISTICAL ANALYSIS

Statistical analysis was carried out using GraphPad Prism software. The two-tailed Student's t test was used to generate statistical significance for pairwise comparisons unless stated otherwise. Survival analysis was performed using the Kaplan–Meier method. The two-sided log-rank test was used to analyze the differences between two group of mice. Statistical details of experiments can be found in the figure legends.

Supplementary Material

Refer to Web version on PubMed Central for supplementary material.

ACKNOWLEDGMENTS

We thank members of the George laboratory and Bo Kyung Alex Seong for helpful discussions. We thank Eric Spooner and the Whitehead Institute Mass Spectrometry Facility and the DFCI Molecular Biology Core for technical support and the Childhood Solid Tumor Network at St. Jude CRH for the PDX models. This work was supported by NIH R01CA148688 (to R.E.G.), Hyundai Hope On Wheels (to R.E.G.), Friends for Life (to R.E.G.), Abraham Fellowship (to H.H.), DFCI/BCH Team Path to the Cure (to H.H.), CIHR PJT-162228 (M.S.I.), and Sebastian's Superheroes and James Fund for Neuroblastoma Research (Sick Kids Foundation) (to M.S.I.).

REFERENCES

Alshareef A, Zhang HF, Huang YH, Wu C, Zhang JD, Wang P, El-Sehemy A, Fares M, and Lai R. (2016). The use of cellular thermal shift assay (CETSA) to study crizotinib resistance in ALK-expressing human cancers. Sci. Rep 6, 33710. [PubMed: 27641368]

Alshareef A, Gupta N, Zhang HF, Wu C, Haque M, and Lai R. (2017). High expression of β-catenin contributes to the crizotinib resistant phenotype in the stem-like cell population in neuroblastoma. Sci. Rep 7, 16863. [PubMed: 29203817]

Barrallo-Gimeno A, and Nieto MA (2005). The Snail genes as inducers of cell movement and survival: implications in development and cancer. Development 132, 3151–3161. [PubMed: 15983400]

Brady SW, Liu Y, Ma X, Gout AM, Hagiwara K, Zhou X, Wang J, Macias M, Chen X, Easton J, et al. (2020). Pan-neuroblastoma analysis reveals age- and signature-associated driver alterations. Nat. Commun 11, 5183. [PubMed: 33056981]

Brew K, and Nagase H. (2010). The tissue inhibitors of metalloproteinases (TIMPs): an ancient family with structural and functional diversity. Biochim. Biophys. Acta 1803, 55–71. [PubMed: 20080133]

Cazes A, Louis-Brennetot C, Mazot P, Dingli F, Lombard B, Boeva V, Daveau R, Cappo J, Combaret V, Schleiermacher G, et al. (2013). Characterization of rearrangements involving the ALK gene reveals a novel truncated form associated with tumor aggressiveness in neuroblastoma. Cancer Res 73, 195–204. [PubMed: 23139213]

Chen Y, Takita J, Choi YL, Kato M, Ohira M, Sanada M, Wang L, Soda M, Kikuchi A, Igarashi T, et al. (2008). Oncogenic mutations of ALK kinase in neuroblastoma. Nature 455, 971–974. [PubMed: 18923524]

De Brouwer S, De Preter K, Kumps C, Zabrocki P, Porcu M, Westerhout EM, Lakeman A, Vandesompele J, Hoebeeck J, Van Maerken T, et al. (2010). Meta-analysis of neuroblastomas reveals a skewed ALK mutation spectrum in tumors with MYCN amplification. Clin. Cancer Res 16, 4353–4362. [PubMed: 20719933]

Debruyne DN, Bhatnagar N, Sharma B, Luther W, Moore NF, Cheung NK, Gray NS, and George RE (2016). ALK inhibitor resistance in ALK(F1174L)-driven neuroblastoma is associated with AXL activation and induction of EMT. Oncogene 35, 3681–3691. [PubMed: 26616860]

Degoutin J, Brunet-de Carvalho N, Cifuentes-Diaz C, and Vigny M. (2009). ALK (anaplastic lymphoma kinase) expression in DRG neurons and its involvement in neuron-Schwann cells interaction. Eur. J. Neurosci 29, 275–286. [PubMed: 19200234]

Di Paolo D, Ambrogio C, Pastorino F, Brignole C, Martinengo C, Carosio R, Loi M, Pagnan G, Emionite L, Cilli M, et al. (2011). Selective therapeutic targeting of the anaplastic lymphoma kinase with liposomal siRNA induces apoptosis and inhibits angiogenesis in neuroblastoma. Mol. Ther 19, 2201–2212. [PubMed: 21829174]

Foster JH, Voss SD, Hall DC, Minard CG, Balis FM, Wilner K, Berg SL, Fox E, Adamson PC, Blaney S, et al. (2021). Activity of crizotinib in patients with ALK-aberrant relapsed/refractory neuroblastoma: a Children's Oncology Group Study (ADVL0912). Clin. Cancer Res, Published online 2 10, 2021. 10.1158.1078-0432.

Fransson S, Hansson M, Ruuth K, Djos A, Berbegall A, Javanmardi N, Abrahamsson J, Palmer RH, Noguera R, Hallberg B, et al. (2015). Intra-genic anaplastic lymphoma kinase (ALK) rearrangements: translocations as a novel mechanism of ALK activation in neuroblastoma tumors. Genes Chromosomes Cancer 54, 99–109. [PubMed: 25251827]

Gautier L, Cope L, Bolstad BM, and Irizarry RA (2004). affy–analysis of Affymetrix GeneChip data at the probe level. Bioinformatics 20, 307–315. [PubMed: 14960456]

George RE, Sanda T, Hanna M, Fröhling S, Luther W 2nd, Zhang J, Ahn Y, Zhou W, London WB, McGrady P, et al. (2008). Activating mutations in ALK provide a therapeutic target in neuroblastoma. Nature 455, 975–978. [PubMed: 18923525]

Guan J, Umapathy G, Yamazaki Y, Wolfstetter G, Mendoza P, Pfeifer K, Mohammed A, Hugosson F, Zhang H, Hsu AW, et al. (2015). FAM150A and FAM150B are activating ligands for anaplastic lymphoma kinase. eLife 4, e09811. [PubMed: 26418745]

Hallberg B, and Palmer RH (2016). The role of the ALK receptor in cancer biology. Ann. Oncol 27 (Suppl 3), iii4–iii15. [PubMed: 27573755]

Hasan MK, Nafady A, Takatori A, Kishida S, Ohira M, Suenaga Y, Hossain S, Akter J, Ogura A, Nakamura Y, et al. (2013). ALK is a MYCN target gene and regulates cell migration and invasion in neuroblastoma. Sci. Rep 3, 3450. [PubMed: 24356251]

Huang D, Rutkowski JL, Brodeur GM, Chou PM, Kwiatkowski JL, Babbo A, and Cohn SL (2000). Schwann cell-conditioned medium inhibits angiogenesis. Cancer Res 60, 5966–5971. [PubMed: 11085514]

Iwahara T, Fujimoto J, Wen D, Cupples R, Bucay N, Arakawa T, Mori S, Ratzkin B, and Yamamoto T. (1997). Molecular characterization of ALK, a receptor tyrosine kinase expressed specifically in the nervous system. Oncogene 14, 439–449. [PubMed: 9053841]

Janoueix-Lerosey I, Lequin D, Brugières L, Ribeiro A, de Pontual L, Combaret V, Raynal V, Puisieux A, Schleiermacher G, Pierron G, et al. (2008). Somatic and germline activating mutations of the ALK kinase receptor in neuroblastoma. Nature 455, 967–970. [PubMed: 18923523]

Jordà M, Olmeda D, Vinyals A, Valero E, Cubillo E, Llorens A, Cano A, and Fabra A. (2005). Upregulation of MMP-9 in MDCK epithelial cell line in response to expression of the Snail transcription factor. J. Cell Sci 118, 3371–3385. [PubMed: 16079281]

Kang Y, Siegel PM, Shu W, Drobnjak M, Kakonen SM, Cordón-Cardo C, Guise TA, and Massagué J. (2003). A multigenic program mediating breast cancer metastasis to bone. Cancer Cell 3, 537–549. [PubMed: 12842083]

Kim Y, Remacle AG, Chernov AV, Liu H, Shubayev I, Lai C, Dolkas J, Shiryaev SA, Golubkov VS, Mizisin AP, et al. (2012). The MMP-9/TIMP-1 axis controls the status of differentiation and function of myelin-forming Schwann cells in nerve regeneration. PLoS ONE 7, e33664. [PubMed: 22438979]

Kioussi C, Briata P, Baek SH, Rose DW, Hamblet NS, Herman T, Ohgi KA, Lin C, Gleiberman A, Wang J, et al. (2002). Identification of a Wnt/Dvl/β-catenin / Pitx2 pathway mediating cell-type-specific proliferation during development. Cell 111, 673–685. [PubMed: 12464179]

Kreitman M, Noronha A, and Yarden Y. (2018). Irreversible modifications of receptor tyrosine kinases. FEBS Lett 592, 2199–2212. [PubMed: 29790151]

Lamant L, Pulford K, Bischof D, Morris SW, Mason DY, Delsol G, and Mariamé B. (2000). Expression of the ALK tyrosine kinase gene in neuroblastoma. Am. J. Pathol 156, 1711–1721. [PubMed: 10793082]

Lamouille S, Xu J, and Derynck R. (2014). Molecular mechanisms of epithelial-mesenchymal transition. Nat. Rev. Mol. Cell Biol 15, 178–196. [PubMed: 24556840]

Levin JI, Chen J, Du M, Hogan M, Kincaid S, Nelson FC, Venkatesan AM, Wehr T, Zask A, DiJoseph J, et al. (2001). The discovery of anthranilic acid-based MMP inhibitors, part 2: SAR of the 5-position and P1(1) groups. Bioorg. Med. Chem. Lett 11, 2189–2192. [PubMed: 11514167]

Li W, Li J, Wu Y, Wu J, Hotchandani R, Cunningham K, McFadyen I, Bard J, Morgan P, Schlerman F, et al. (2009). A selective matrix metalloprotease 12 inhibitor for potential treatment of chronic obstructive pulmonary disease (COPD): discovery of (S)-2-(8-(methoxycarbonylamino)dibenzo[b,d] furan-3-sulfonamido)-3-methylbutanoic acid (MMP408). J. Med. Chem 52, 1799–1802. [PubMed: 19278250]

Lin CY, Tsai PH, Kandaswami CC, Lee PP, Huang CJ, Hwang JJ, and Lee MT (2011). Matrix metalloproteinase-9 cooperates with transcription factor Snail to induce epithelial-mesenchymal transition. Cancer Sci 102, 815–827. [PubMed: 21219539]

Liu X, Fridman JS, Wang Q, Caulder E, Yang G, Covington M, Liu C, Marando C, Zhuo J, Li Y, et al. (2006). Selective inhibition of ADAM metalloproteases blocks HER-2 extracellular domain (ECD) cleavage and potentiates the anti-tumor effects of trastuzumab. Cancer Biol. Ther 5, 648–656. [PubMed: 16627988]

Lovén J, Orlando DA, Sigova AA, Lin CY, Rahl PB, Burge CB, Levens DL, Lee TI, and Young RA (2012). Revisiting global gene expression analysis. Cell 151, 476–482. [PubMed: 23101621]

Maetzel D, Denzel S, Mack B, Canis M, Went P, Benk M, Kieu C, Papior P, Baeuerle PA, Munz M, and Gires O. (2009). Nuclear signalling by tumour-associated antigen EpCAM. Nat. Cell Biol 11, 162–171. [PubMed: 19136966]

Meng W, and Takeichi M. (2009). Adherens junction: molecular architecture and regulation. Cold Spring Harb. Perspect. Biol 1, a002899. [PubMed: 20457565]

Miller MA, Oudin MJ, Sullivan RJ, Wang SJ, Meyer AS, Im H, Frederick DT, Tadros J, Griffith LG, Lee H, et al. (2016). Reduced Proteolytic Shedding of Receptor Tyrosine Kinases Is a Post-Translational Mechanism of Kinase Inhibitor Resistance. Cancer Discov 6, 382–399. [PubMed: 26984351]

Molina MA, Codony-Servat J, Albanell J, Rojo F, Arribas J, and Baselga J. (2001). Trastuzumab (herceptin), a humanized anti-Her2 receptor monoclonal antibody, inhibits basal and activated Her2 ectodomain cleavage in breast cancer cells. Cancer Res 61, 4744–4749. [PubMed: 11406546]

Moog-Lutz C, Degoutin J, Gouzi JY, Frobert Y, Brunet-de Carvalho N, Bureau J, Créminon C, and Vigny M. (2005). Activation and inhibition of anaplastic lymphoma kinase receptor tyrosine kinase by monoclonal antibodies and absence of agonist activity of pleiotrophin. J. Biol. Chem 280, 26039–26048. [PubMed: 15886198]

Morris SW, Kirstein MN, Valentine MB, Dittmer KG, Shapiro DN, Saltman DL, and Look AT (1994). Fusion of a kinase gene, ALK, to a nucleolar protein gene, NPM, in non-Hodgkin's lymphoma. Science 263, 1281–1284. [PubMed: 8122112]

Mossé YP, Laudenslager M, Longo L, Cole KA, Wood A, Attiyeh EF, Laquaglia MJ, Sennett R, Lynch JE, Perri P, et al. (2008). Identification of ALK as a major familial neuroblastoma predisposition gene. Nature 455, 930–935. [PubMed: 18724359]

Motegi A, Fujimoto J, Kotani M, Sakuraba H, and Yamamoto T. (2004). ALK receptor tyrosine kinase promotes cell growth and neurite outgrowth. J. Cell Sci 117, 3319–3329. [PubMed: 15226403]

Mourali J, Bénard A, Lourenço FC, Monnet C, Greenland C, Moog-Lutz C, Racaud-Sultan C, Gonzalez-Dunia D, Vigny M, Mehlen P, et al. (2006). Anaplastic lymphoma kinase is a dependence receptor whose proapoptotic functions are activated by caspase cleavage. Mol. Cell. Biol 26, 6209–6222. [PubMed: 16880530]

O'Bryan JP, Fridell YW, Koski R, Varnum B, and Liu ET (1995). The transforming receptor tyrosine kinase, Axl, is post-translationally regulated by proteolytic cleavage. J. Biol. Chem 270, 551–557. [PubMed: 7822279]

Okubo J, Takita J, Chen Y, Oki K, Nishimura R, Kato M, Sanada M, Hiwatari M, Hayashi Y, Igarashi T, and Ogawa S. (2012). Aberrant activation of ALK kinase by a novel truncated form ALK protein in neuroblastoma. Oncogene 31, 4667–4676. [PubMed: 22249260]

Osajima-Hakomori Y, Miyake I, Ohira M, Nakagawara A, Nakagawa A, and Sakai R. (2005). Biological role of anaplastic lymphoma kinase in neuroblastoma. Am. J. Pathol 167, 213–222. [PubMed: 15972965]

Passoni L, Longo L, Collini P, Coluccia AM, Bozzi F, Podda M, Gregorio A, Gambini C, Garaventa A, Pistoia V, et al. (2009). Mutation-independent anaplastic lymphoma kinase overexpression in poor prognosis neuroblastoma patients. Cancer Res 69, 7338–7346. [PubMed: 19723661]

Ponomarev V, Doubrovin M, Serganova I, Vider J, Shavrin A, Beresten T, Ivanova A, Ageyeva L, Tourkova V, Balatoni J, et al. (2004). A novel triple-modality reporter gene for whole-body fluorescent, bioluminescent, and nuclear noninvasive imaging. Eur. J. Nucl. Med. Mol. Imaging 31, 740–751. [PubMed: 15014901]

Ran FA, Hsu PD, Lin CY, Gootenberg JS, Konermann S, Trevino AE, Scott DA, Inoue A, Matoba S, Zhang Y, and Zhang F. (2013). Double nicking by RNA-guided CRISPR Cas9 for enhanced genome editing specificity. Cell 154, 1380–1389. [PubMed: 23992846]

Reshetnyak AV, Murray PB, Shi X, Mo ES, Mohanty J, Tome F, Bai H, Gunel M, Lax I, and Schlessinger J. (2015). Augmentor a and b (FAM150) are ligands of the receptor tyrosine kinases ALK and LTK: Hierarchy and specificity of ligand-receptor interactions. Proc. Natl. Acad. Sci. USA 112, 15862–15867. [PubMed: 26630010]

Rio C, Buxbaum JD, Peschon JJ, and Corfas G. (2000). Tumor necrosis factor-alpha-converting enzyme is required for cleavage of erbB4/HER4. J. Biol. Chem 275, 10379–10387. [PubMed: 10744726]

Schelter F, Kobuch J, Moss ML, Becherer JD, Comoglio PM, Boccaccio C, and Krüger A. (2010). A disintegrin and metalloproteinase-10 (ADAM-10) mediates DN30 antibody-induced shedding of the met surface receptor. J. Biol. Chem 285, 26335–26340. [PubMed: 20554517]

Schneider CA, Rasband WS, and Eliceiri KW (2012). NIH Image to ImageJ: 25 years of image analysis. Nat. Methods 9, 671–675. [PubMed: 22930834]

Schönherr C, Ruuth K, Kamaraj S, Wang CL, Yang HL, Combaret V, Djos A, Martinsson T, Christensen JG, Palmer RH, and Hallberg B. (2012). Anaplastic Lymphoma Kinase (ALK) regulates initiation of transcription of MYCN in neuroblastoma cells. Oncogene 31, 5193–5200. [PubMed: 22286764]

Schulte JH, Bachmann HS, Brockmeyer B, Depreter K, Oberthur A, Ackermann S, Kahlert Y, Pajtler K, Theissen J, Westermann F, et al. (2011). High ALK receptor tyrosine kinase expression supersedes ALK mutation as a determining factor of an unfavorable phenotype in primary neuroblastoma. Clin. Cancer Res 17, 5082–5092. [PubMed: 21632861]

Seong BK, Fathers KE, Hallett R, Yung CK, Stein LD, Mouaaz S, Kee L, Hawkins CE, Irwin MS, and Kaplan DR (2017). A metastatic mouse model identifies genes that regulate neuroblastoma metastasis. Cancer Res 77, 696–706. [PubMed: 27899382]

Shah MA, Starodub A, Sharma S, Berlin J, Patel M, Wainberg ZA, Chaves J, Gordon M, Windsor K, Brachmann CB, et al. (2018). Andeca-liximab/GS-5745 alone and combined with mFOLFOX6 in advanced gastric and gastroesophageal junction adenocarcinoma: results from a phase I study. Clin. Cancer Res 24, 3829–3837. [PubMed: 29691300]

Shimada H, Chatten J, Newton WA Jr., Sachs N, Hamoudi AB, Chiba T, Marsden HB, and Misugi K. (1984). Histopathologic prognostic factors in neuroblastic tumors: definition of subtypes of ganglioneuroblastoma and an age-linked classification of neuroblastomas. J. Natl. Cancer Inst 73, 405–416. [PubMed: 6589432]

Shoval I, Ludwig A, and Kalcheim C. (2007). Antagonistic roles of full-length N-cadherin and its soluble BMP cleavage product in neural crest delamination. Development 134, 491–501. [PubMed: 17185320]

Smyth GK, Yang YH, and Speed T. (2003). Statistical issues in cDNA microarray data analysis. Methods Mol. Biol 224, 111–136. [PubMed: 12710670]

Song J, Tan H, Perry AJ, Akutsu T, Webb GI, Whisstock JC, and Pike RN (2012). PROSPER: an integrated feature-based tool for predicting protease substrate cleavage sites. PLoS ONE 7, e50300. [PubMed: 23209700]

Souttou B, Carvalho NB, Raulais D, and Vigny M. (2001). Activation of anaplastic lymphoma kinase receptor tyrosine kinase induces neuronal differentiation through the mitogen-activated protein kinase pathway. J. Biol. Chem 276, 9526–9531. [PubMed: 11121404]

Stoyanova T, Goldstein AS, Cai H, Drake JM, Huang J, and Witte ON (2012). Regulated proteolysis of Trop2 drives epithelial hyperplasia and stem cell self-renewal via β-catenin signaling. Genes Dev 26, 2271–2285. [PubMed: 23070813]

Tanjore H, and Kalluri R. (2006). The role of type IV collagen and basement membranes in cancer progression and metastasis. Am. J. Pathol 168, 715–717. [PubMed: 16507886]

Thiery JP, Acloque H, Huang RY, and Nieto MA (2009). Epithelial-mesenchymal transitions in development and disease. Cell 139, 871–890. [PubMed: 19945376]

Valenta T, Hausmann G, and Basler K. (2012). The many faces and functions of β-catenin. EMBO J 31, 2714–2736. [PubMed: 22617422]

van Veelen W, Le NH, Helvensteijn W, Blonden L, Theeuwes M, Bakker ER, Franken PF, van Gurp L, Meijlink F, van der Valk MA, et al. (2011). β-catenin tyrosine 654 phosphorylation increases Wnt signalling and intestinal tumorigenesis. Gut 60, 1204–1212. [PubMed: 21307168]

Vandooren J, Van den Steen PE, and Opdenakker G. (2013). Biochemistry and molecular biology of gelatinase B or matrix metalloproteinase-9 (MMP-9): the next decade. Crit. Rev. Biochem. Mol. Biol 48, 222–272. [PubMed: 23547785]

Xiang FL, Fang M, and Yutzey KE (2017). Loss of β-catenin in resident cardiac fibroblasts attenuates fibrosis induced by pressure overload in mice. Nat. Commun 8, 712. [PubMed: 28959037]

Zhang Z, Lee JC, Lin L, Olivas V, Au V, LaFramboise T, Abdel-Rahman M, Wang X, Levine AD, Rho JK, et al. (2012). Activation of the AXL kinase causes resistance to EGFR-targeted therapy in lung cancer. Nat. Genet 44, 852–860. [PubMed: 22751098]

Zirkel A, Lederer M, Stöhr N, Pazaitis N, and Hüttelmaier S. (2013). IGF2BP1 promotes mesenchymal cell properties and migration of tumor-derived cells by enhancing the expression of LEF1 and SNAI2 (SLUG). Nucleic Acids Res 41, 6618–6636. [PubMed: 23677615]

Highlights

- ALK extracellular domain (ECD) cleavage occurs at Asn 654-Leu655
- ECD cleavage mediates neuroblastoma (NB) cell migration
- Cleavage inhibition leads to downregulated nuclear β-catenin and EMT gene signatures
- ECD cleavage is caused by MMP-9 whose inhibition decreases NB cell migration

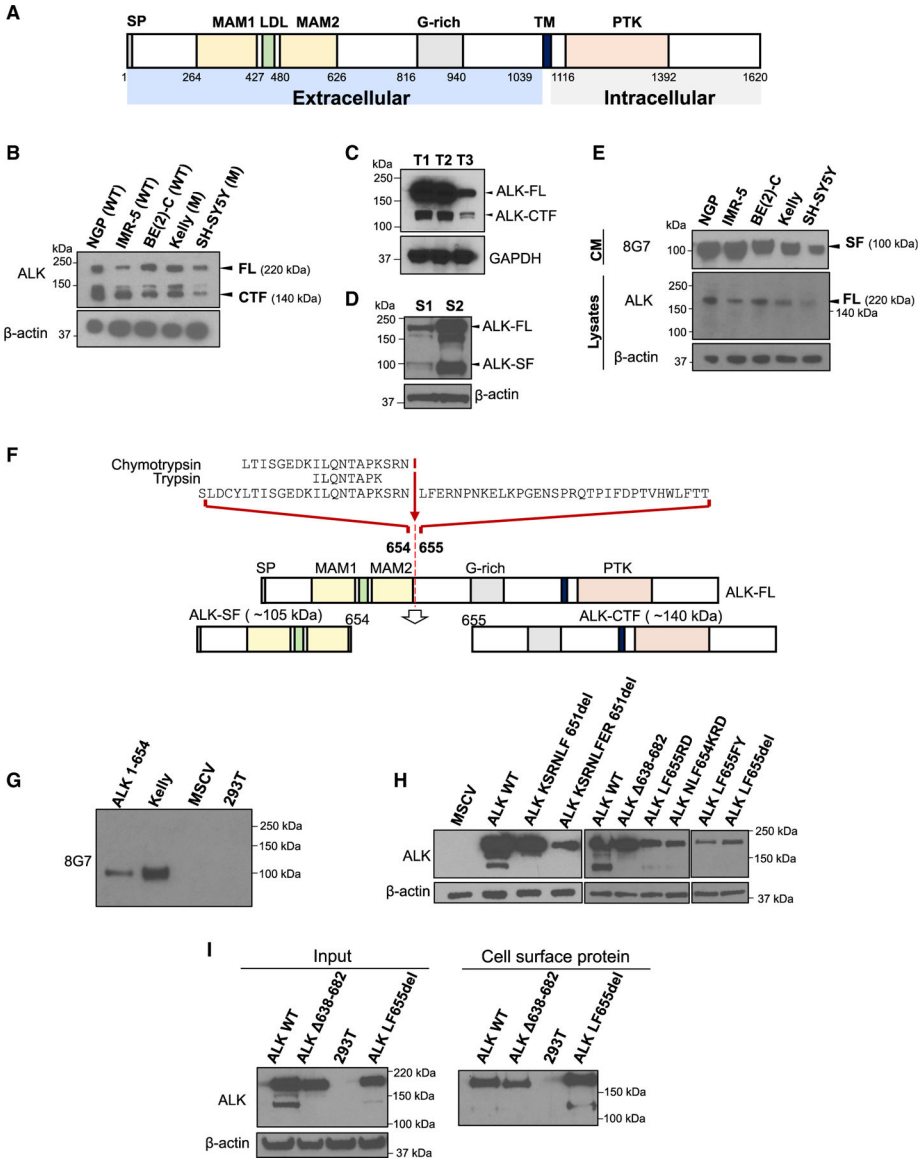

Figure 1. ALK undergoes ECD cleavage at Asn654-Leu655

(A) Schematic illustration of the structure of ALK. TM, transmembrane; SP, signal peptide; LDL, low-density lipoprotein receptor domain; MAM, meprin, A-5 protein and receptor protein-tyrosine phosphatase mu domain; G-rich, glycine-rich; PTK, protein tyrosine kinase domains. Numbers indicate amino acid positions. Dashed gray line indicates putative ligand-binding region.

(B) Western blot (WB) analysis of ALK expression using a C-terminal anti-ALK antibody (C26G7) in the indicated NB cell lysates. WT, wild-type; M, ALK-mutated; FL, full-length ALK; CTF, membrane-bound C-terminal ALK fragment here and throughout the figure.

(C) WB analysis of ALK expression in PDX NB models using C-terminal anti-ALK antibodies. Lanes T1 and T2 (tumor sample SJNBL046148_X1 in duplicate); lane T3 (SJNBL013761_1).

(D) WB analysis of ALK expression in brain tissue from P0 (S1) and P7 (S2) mice using an N-terminal anti-ALK antibody.
(E) WB analysis of ALK expression in conditioned media (CM) or cell lysates of NB cells with the N-terminal 8G7 anti-ALK antibody. SF, secreted extracellular fragment.
(F) Schematic illustration of the putative ECD cleavage site inferred from LC-MS/MS analysis. The red arrow indicates the cleavage position between amino acids 654 and 655.
(G) WB analysis of ALK in cell lysates from 293T cells engineered to express the shed fragment (ALK1–654) and CM from Kelly NB cells that express full-length, cleaved ALK using the 8G7 antibody. Negative controls, empty vector-expressing (MSCV) and untransfected cells (293T).
(H) WB analysis of ALK in 293T cells expressing wild-type (ALK WT) or engineered ALK variants. Negative controls, cells expressing the MSCV vector .
(I) Cell surface protein analysis of ALK in 293T cells engineered to express the indicated WT or mutant constructs. Cell surface proteins were labeled with sulfo-NHS-SS-biotin and isolated with streptavidin beads.
See also Figures S1, S2, and S3.

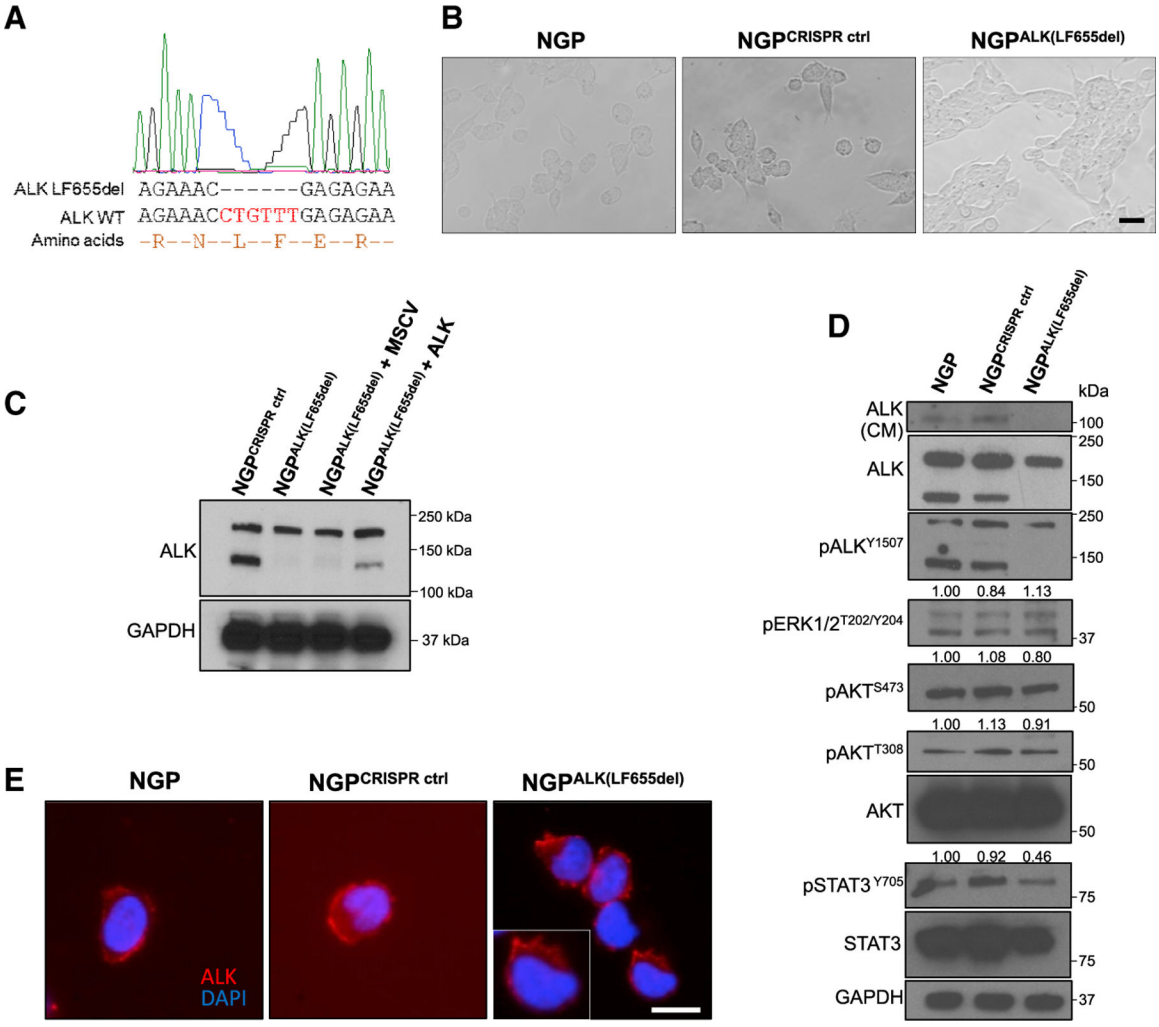

Figure 2. Insertion of the LF655del mutation inhibits ALK ECD cleavage in NB cells

(A) Electropherogram of the region in which the ALK LF655del mutation was introduced through biallelic CRISPR-cas9 editing.

(B) Representative phase contrast microscopy images of NGP NB cells in which the ECD cleavage site was genomically altered using CRISPR-cas9 editing ($NGP^{ALK(LF655del)}$). Controls, unedited NGP cells (NGP) and vector control ($NGP^{CRISPR\ ctrl}$) cells. Scale bar, 25 μm.

(C) WB analysis of ALK expression in $NGP^{ALK(LF655del)}$ or $NGP^{CRISPR\ ctrl}$ cells in which ALK WT (+ALK) or empty vector (+MSCV) was expressed. GAPDH was used as the loading control throughout.

(D) WB analysis of ALK and the indicated proteins in conditioned media (CM) or lysates from the same cells as in (B). The same cell lysates were used to perform the WB analysis shown in Figure 5F (in the same experiment); hence, ALK and GAPDH are the same for both blots.

(E) Representative immunofluorescence (IF) images of ALK expression in the same cells as in (B). Nuclei were stained with DAPI. Scale bar,10 μm.

See also Figure S4.

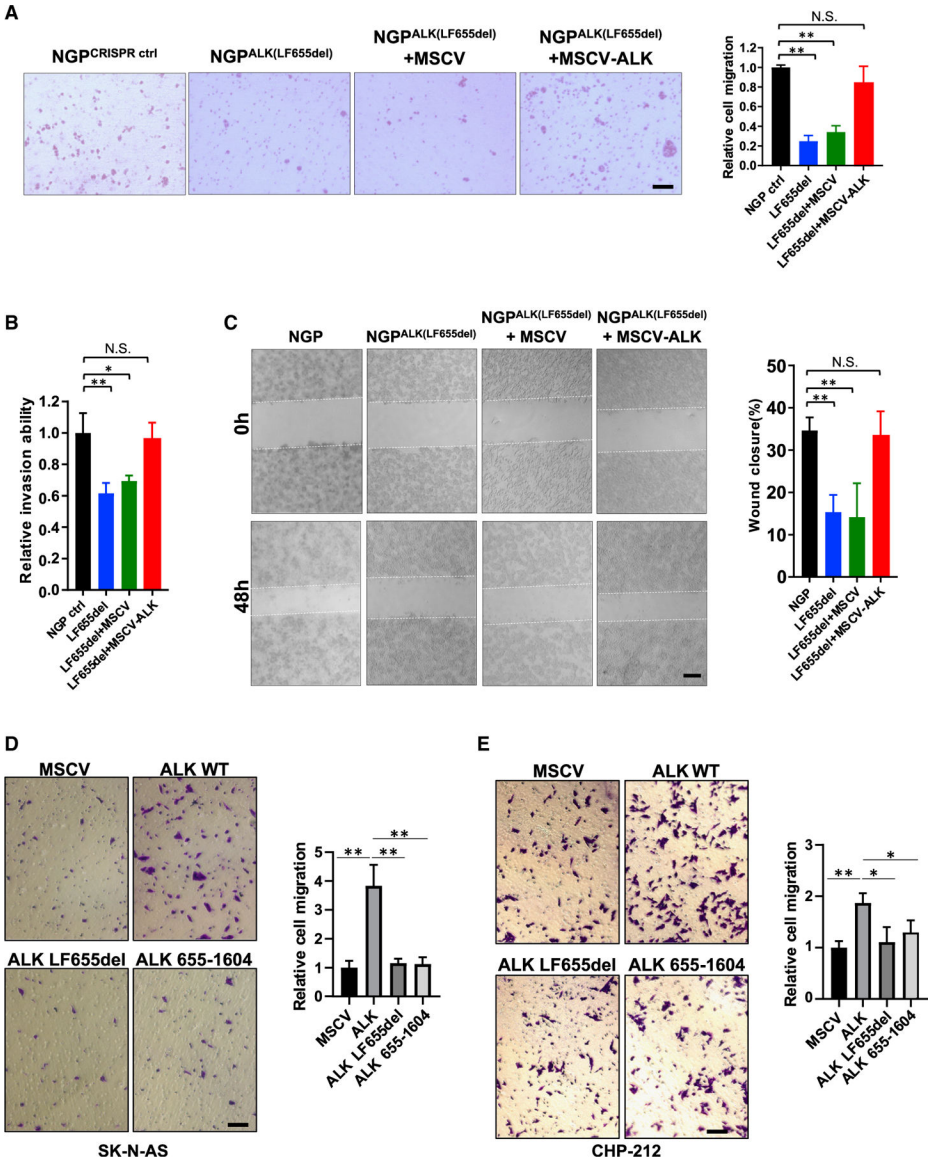

Figure 3. Inhibition of ALK ECD cleavage suppresses migration and invasion of NB cells

(A) Representative crystal violet-stained images of transwell migration assays of the indicated cells (left). Scale bar, 100 μm. Quantification of cell migration determined by counting the number of migratory cells per field and calculating the relative numbers of modified to control cells (right). Values are reported as means ± SD; **p < 0.01, n = 3.

(B) Quantification of cell invasion in NGP cells in which cleavage was inhibited through genome editing (LF655del) versus control cells (NGP ctrl) and in cells in which ALK WT (LF655del + MSCV-ALK) or control vector (LF655del + MSCV) were expressed. Invasive capacity was quantified as means ± SD, n = 3; *p < 0.05, **p < 0.01.

(C) Representative phase-contrast microscopy images of wound healing in the indicated NGP cells at 0 and 48 h (left). Scale bar, 500 μm. Percentage of wound closure depicted as means ± SD, n = 12; **p < 0.01 (right).

(D and E) Crystal-violet-stained images of transwell migration of SK-N-AS (D) and CHP-212 (E) NB cells expressing the indicated ALK proteins (left). Empty vector, MSCV was used as a negative control. Scale bars, 100 μm. Quantification of cell migration (right). Values are means ± SD; *$p < 0.05$, **$p < 0.01$, $n = 3$ for each panel.
See also Figures S5 and S6.

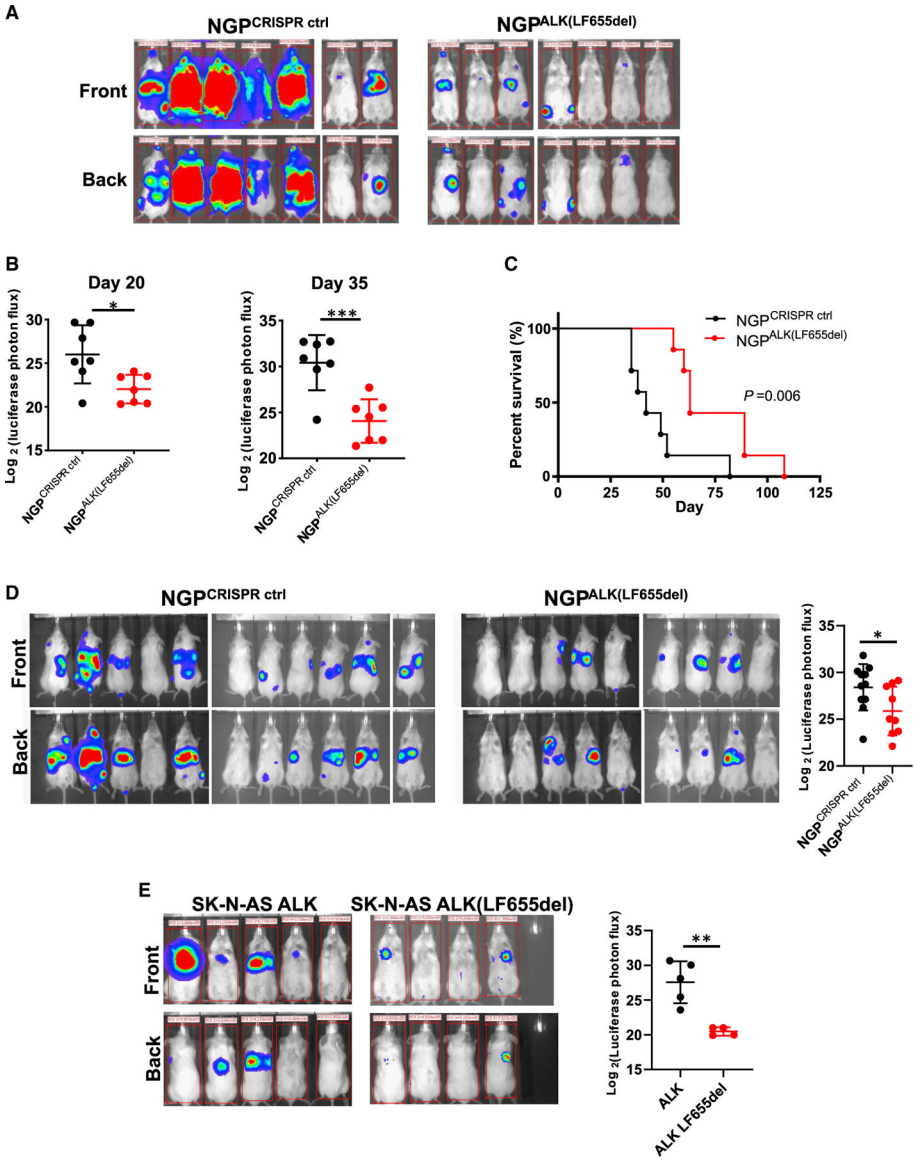

Figure 4. Inhibition of ALK ECD cleavage reduces NB cell migration *in vivo*

(A) Representative bioluminescence images (BLIs) of NOD/SCID mice 35 days after intracardiac injection of the indicated luciferase-labeled NGP NB cells (1×10^5 cells per animal).

(B) Comparison of bioluminescence in the animals described in (A) at day 20 and day 35 after injection. Bioluminescence was quantified as photon flux per second over time. The data are presented as means ± SEM, n = 7 mice per group; *p < 0.05, ***p < 0.001.

(C) Kaplan-Meier analysis of overall survival of mice in (A). Significance was calculated by the log-rank test (p = 0.006; n = 7 per group).

(D) Representative BLIs of NOD/SCID mice 42 days after tail-vein injection of the indicated luciferase-labeled NGP NB cells (5×10^5 per animal) (left). Comparison of bioluminescence quantified as in (B) at day 42 after injection (right). Data are presented as means ± SEM, *p < 0.05; n = 11 ($NGP^{CRISPR\ ctrl}$), n = 9 ($NGP^{ALK(LF655del)}$).

(E) Representative BLIs of NOD/SCID mice 46 days after intracardiac injection of 1×10^5 luciferase-labeled SK-N-AS NB cells expressing ALK WT (n = 5) and the ALK LF655del CSM (n = 4) (left). Comparison of bioluminescence at day 46 (right). Data are presented as means ± SEM, **p < 0.01.

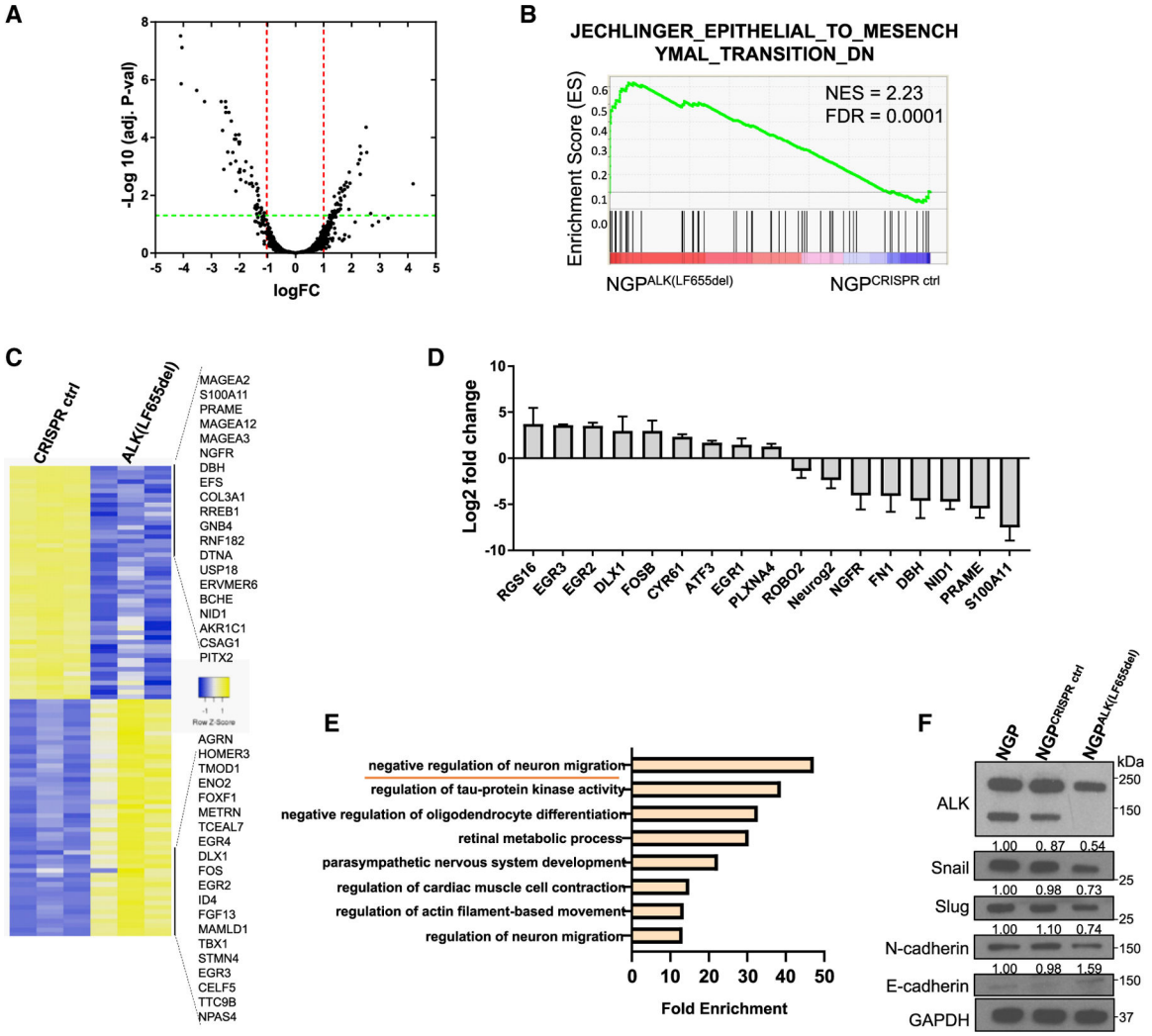

Figure 5. Inhibition of ALK ECD cleavage leads to a downregulated EMT signature

(A) Volcano plot showing gene-expression changes between $NGP^{CRISPR\ ctrl}$ and $NGP^{ALK(LF655del)}$ cells. Downregulated transcripts, 0.26%; upregulated transcripts, 0.21% (false discovery rate [FDR] < 0.05; fold change > 2). The x axis represents the fold change in gene expression (log_2 ratio of $NGP^{ALK(LF655del)}$ versus $NGP^{CRISPR\ ctrl}$) and the y axis, the $-log_{10}$ (adjusted p value). Dashed red lines denote the selected 2-fold change cutoff, whereas the green line denotes the selected p value cutoff.

(B) GSEA plot of an EMT signature in $NGP^{ALK(LF655del)}$ versus $NGP^{CRISPR\ ctrl}$ cells. NES, normalized enrichment scores.

(C) Heatmap of the top 100 genes differentially expressed between $NGP^{ALK(LF655del)}$ cells and $NGP^{CRISPR\ ctrl}$ cells. The highest ranked upregulated (yellow) and downregulated (blue) genes are listed.

(D) Quantitative real-time PCR analysis of selected differentially expressed genes in $NGP^{ALK(LF655del)}$ versus $NGP^{CRISPR\ ctrl}$ cells. Data were normalized to GAPDH. Quantification is shown as log_2-normalized fold change. Error bars represent means ± SD (n = 3 replicates).

(E) GO analysis of significantly up- or downregulated genes in $NGP^{ALK(LF655del)}$ versus $NGP^{CRISPR\ ctrl}$ cells. ‘‘Negative regulation of neuron migration’’ comprised the most-enriched category in $NGP^{ALK(LF655del)}$ cells (> 40-fold; $p = 3.93e^{-6}$).
(F) WB analysis of ALK and the indicated EMT markers in $NGP^{ALK(LF655del)}$ versus $NGP^{CRISPR\ ctrl}$ cells. Unedited cells (NGP) were used as a reference. GAPDH was used as a loading control.

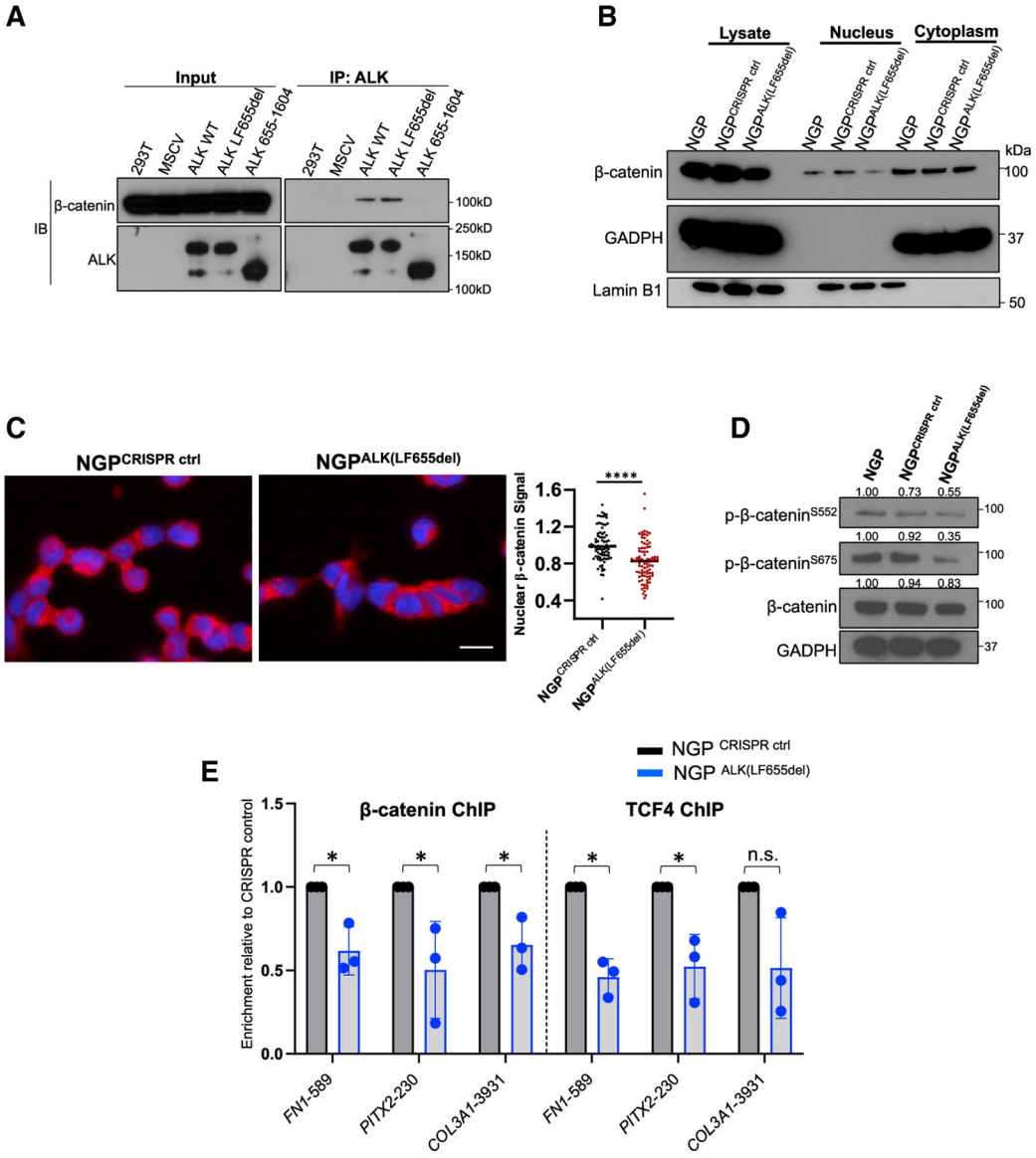

Figure 6. ALK ECD cleavage affects EMT gene expression through changes in nuclear β-catenin localization

(A) WB analysis of co-immunoprecipitated (co-IP) ALK and β-catenin in 293T cells engineered to express WT or the indicated mutant ALK constructs and immunoprecipitated with an anti-ALK C-terminal antibody. IB, immunoblot.

(B) WB analysis of β-catenin in subcellular fractions and total cell lysates of the indicated NB cells. Lamin B1 expression was used as a control for the nuclear fraction.

(C) IF analysis of β-catenin expression in the indicated cells (left). Nuclei are stained with DAPI (blue). Red, β-catenin. Scale bar,10 μm. Quantification of β-catenin signal in the nucleus (right); ****$p < 0.0001$, $n = 84$ cells per group; two independent replicates; Student t test.

(D) WB analysis of total and phospho-β-catenin in total cell lysates of the indicated cells. GAPDH used as a loading control.

(E) ChIP-qPCR analysis of β-catenin and TCF4 occupancy at putative TCF4/LEF/TCF-4E binding sites of the indicated gene promoters in $NGP^{CRISPR\ ctrl}$ and $NGP^{ALK(LF655del)}$ cells. Numbers on the x axis indicate the genomic locations of the putative TCF4 sites with reference to the transcription start sites. Data represent means ± SD, n = 3 biological replicates (blue dots). *$p < 0.05$; one-tailed Welch's t test.

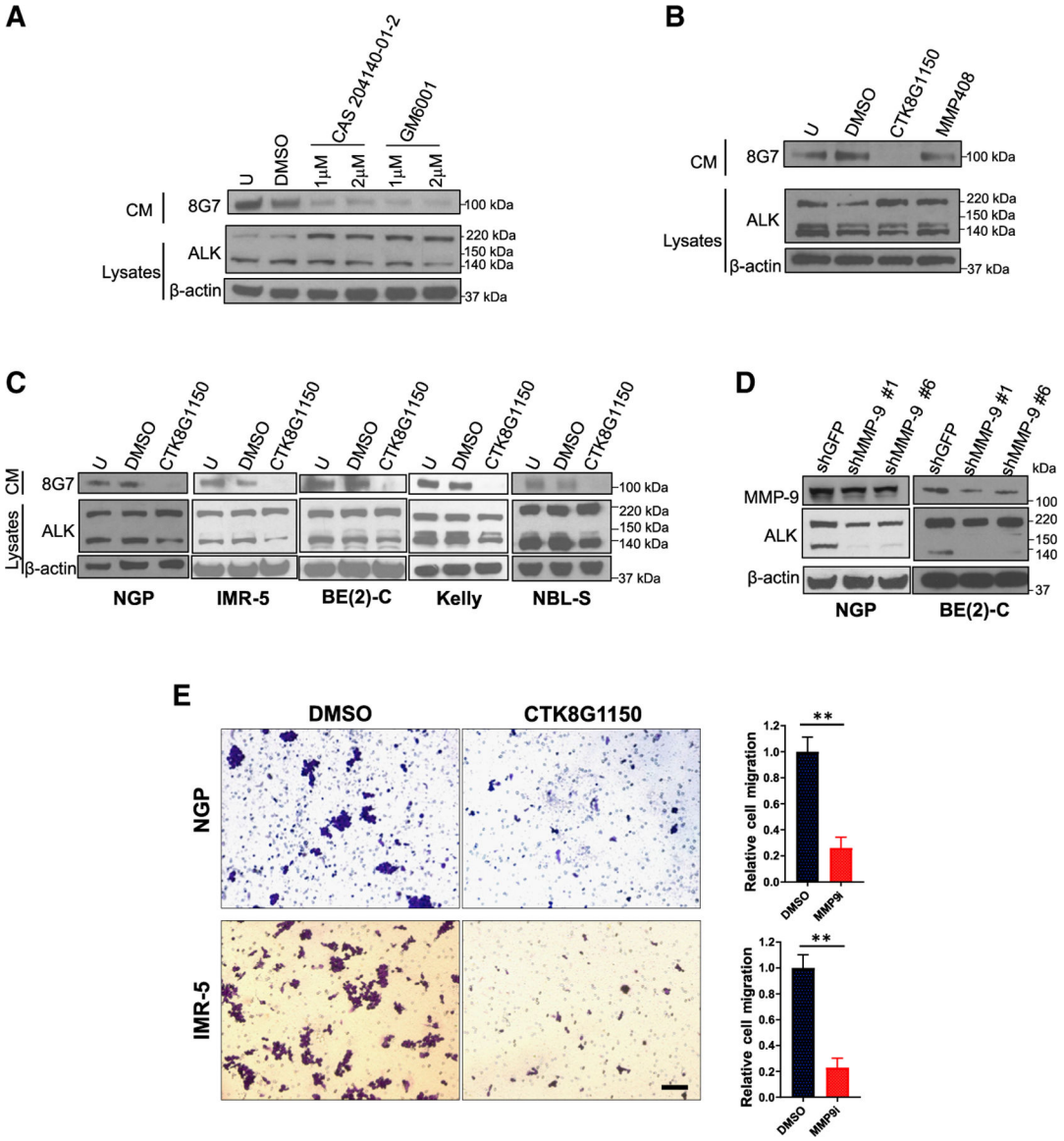

Figure 7. ALK ECD cleavage is mediated by MMP-9 whose inhibition suppresses cell migration

(A) WB analysis of ALK expression in lysates and CM of NGP cells treated with the broad-spectrum protease inhibitor GM6001 and the MMP-9/13 inhibitor CAS 204140–01-2 at the indicated doses, for 12 h. Untreated (U) or DMSO-treated cells were used as controls. The 8G7 N-terminal anti-ALK antibody was used to detect the shed fragment in CM and a C-terminal anti-ALK antibody used for the cell lysates in this and subsequent panels. β-actin is used as a loading control throughout.

(B) WB analysis of ALK expression in NGP cells treated with the MMP-9 (CTK8G1150) and MMP-3/12/13 (MMP408) inhibitors (2 μM × 12 h).

(C) WB analysis of ALK expression in the indicated NB cell lines treated with or without CTK8G1150 (2 μM × 12 h).

(D) WB analysis of MMP-9 and ALK expression in NGP and BE (2)-C NB cells expressing either a control shRNA (shGFP) or two different shRNAs against MMP-9.

(E) Crystal-violet-stained images of NGP and IMR-5 NB cells treated with CTK8G1150 (2 μM) or DMSO for 16 h and then subjected to transwell migration assays for 48 h (left). Scale bar, 100 μm. Quantification of migration (right) reported as means ± SD; **$p < 0.01$, $n = 4$.

See also Figure S7.